JGR Planets

RESEARCH ARTICLE
10.1029/2024JE008891

Key Points:

- The Greenheugh pediment/Siccar Point group unconformity affected diagenesis in Gale crater
- Glen Torridon has a paucity of diagenetic features suggesting that the clay mineral-rich nature of that area impeded diagenetic fluid flow
- The nature of diagenetic features changes abruptly at the Jura to Knockfarril Hill and Knockfarril Hill to Glasgow member transitions

Supporting Information:

Supporting Information may be found in the online version of this article.

Correspondence to:

R. Y. Sheppard,
rsheppard@psi.edu

Citation:

Ando, J., Sheppard, R. Y., Bryk, A. B., Sun, V., Seeger, C. H., Fraeman, A. A., et al. (2025). Diagenetic features reveal the influence of the Greenheugh pediment on the alteration history of Gale crater, Mars. *Journal of Geophysical Research: Planets*, *130*, e2024JE008891. https://doi.org/10.1029/2024JE008891

Received 19 DEC 2024
Accepted 21 MAR 2025

Author Contributions:

Conceptualization: Rachel Y. Sheppard, Vivian Sun, Abigail A. Fraeman
Data curation: Jordan Ando, Rachel Y. Sheppard
Formal analysis: Jordan Ando, Rachel Y. Sheppard
Funding acquisition: Abigail A. Fraeman
Investigation: Jordan Ando, Rachel Y. Sheppard, Alexander B. Bryk, Linda Kah
Methodology: Rachel Y. Sheppard, Abigail A. Fraeman
Project administration: Rachel Y. Sheppard
Supervision: Rachel Y. Sheppard, Abigail A. Fraeman

Diagenetic Features Reveal the Influence of the Greenheugh Pediment on the Alteration History of Gale Crater, Mars

Jordan Ando[1], Rachel Y. Sheppard[2,3], Alexander B. Bryk[4], Vivian Sun[5], Christina H. Seeger[6], Abigail A. Fraeman[5], Alivia M. Eng[7], Linda Kah[8], and Amanda N. Rudolph[9]

[1]University of Hawai'i, Honolulu, HI, USA, [2]Planetary Science Institute, Tucson, AZ, USA, [3]Institut d'Astrophysique Spatiale, Université Paris-Saclay, CNRS, Orsay, France, [4]University of California Berkeley, Berkeley, CA, USA, [5]Jet Propulsion Laboratory, California Institute of Technology, Pasadena, CA, USA, [6]California Institute of Technology, Pasadena, CA, USA, [7]Georgia Institute of Technology, Atlanta, GA, USA, [8]University of Tennessee Knoxville, Knoxville, TN, USA, [9]Center for Earth and Planetary Studies, National Air and Space Museum, Smithsonian Institution, Washington, DC, USA

Abstract We investigate the nature of diagenetic features encountered by the Curiosity rover within Mount Sharp from sols 1900–3,049. Using Curiosity's Mars Hand Lens Imager and Mast Camera (Mastcam), we classify diagenetic features into established morphological categories and assess their spatial distribution, density, and size. Our analysis reveals variations in diagenetic feature density and morphology linked to stratigraphic boundaries and proximity to the Greenheugh Pediment unconformity, highlighting the role of diagenetic fluids in shaping these features. We find a reduction in diagenetic features at the Jura to Knockfarril Hill member boundary, a spike in feature abundance at the Knockfarril Hill to Glasgow member boundary, and a strong statistical relationship between feature abundance and vertical distance from the Greenheugh Pediment. These trends point to a dynamic history of diagenetic fluid flow, influenced by variations in porosity, permeability, and structural controls, including the presence of the Pediment.

Plain Language Summary We track the morphology, size, and within-scene density of post-depositional (diagenetic) features on Mount Sharp in Gale crater, as a way to characterize subsurface fluid flow. To study these changes, we analyzed images taken by Curiosity's Mars Hand Lens Imager (MAHLI) and Mast Camera (Mastcam). MAHLI provided views of rock textures and mineral deposits, while Mastcam helped map their distribution over larger areas. The results show that water moved differently through different layers of rock, revealing a more complex history of groundwater activity in the Gale Crater than previously thought. We found that the Greenheugh Pediment (a broad, sloping surface that cuts across older layers of rock) affected the distribution of these features. Below the Pediment surface are distinct stratigraphic regions, including the Knockfarril Hill and Glasgow members, which formed in ancient lake or river environments. We find that in the Knockfarril Hill region, very few diagenetic features were present, possibly because the rocks contained many clay minerals that acted as a barrier to water flow (aquitard). In contrast, in the Glasgow region, there was a sudden increase in diagenetic features, suggesting that groundwater had a much greater effect. Features abundance is strongly correlated with vertical distance from the Greenheugh Pediment.

1. Introduction

1.1. Understanding Diagenesis in Gale Crater

Mars' Gale crater is a ∼3.8 Ga old crater that was subsequently filled by a combination of lacustrine, fluvial, and aeolian sediments (Vasavada, 2022 and references therein). Today, some of the fill deposits that remain make up Aeolis Mons, informally known as Mount Sharp, a 5 km tall sedimentary mound at Gale crater's center. Mount Sharp's stratigraphy preserves evidence about Mars' habitable past and is hypothesized to provide a window into the planet's climate history (Milliken et al., 2010; Vasavada, 2022). For this reason, Gale crater was chosen as the landing site for the Mars Science Laboratory (MSL) Curiosity rover, which has been approaching and ascending Mount Sharp for over 4300 sols. Curiosity uses its payload to study the geology and geochemistry of Mount Sharp in order to assess whether it preserves past habitable environments and document how these environments changed over time. Because Mount Sharp is of geologic interest as a record of Martian climate and habitability through time, determining the mutability of the rock record after its original deposition is important. Diagenesis

Visualization: Jordan Ando, Rachel Y. Sheppard
Writing – original draft: Jordan Ando, Rachel Y. Sheppard
Writing – review & editing: Rachel Y. Sheppard, Alexander B. Bryk, Christina H. Seeger, Abigail A. Fraeman, Alivia M. Eng, Amanda N. Rudolph

can overprint primary chemical and mineralogical trends and obscure primary sedimentologic structures at any time between early lithification and periods of late-stage groundwater flow.

In this paper, we continue the systematic documentation and classification of diagenetic features in Mount Sharp by applying the same methodologies of Sun et al. (2019) to Curiosity's observations from sols 1900–3049 (Figure 1). This date range includes parts of Vera Rubin ridge (VRR), as well as Glen Torridon. Not only do these geologic features host a variety of diagenetic features, but Glen Torridon also documents a transition from a primarily low-energy lacustrine environment to a fluvial lake-margin setting (Bennett et al., 2021, 2022; Caravaca et al., 2022; Cardenas et al., 2022; Edgar et al., 2020; Fedo et al., 2022). Characterizing the morphologies and abundances of diagenetic features in this region will help to further untangle Mount Sharp's complex diagenetic history. We adopt the same general morphological classes as Sun et al. (2019), in order to extend their analyses of late-stage diagenetic episodes in Mount Sharp. Understanding the timing and number of late-stage diagenetic events that occurred will inform our understanding of the history of liquid water at Gale crater, and with it, Mars' potential for habitability.

1.2. Diagenesis in Mount Sharp Stratigraphy and Major Features

The stratigraphic units covered by the sol range of this work are shown in Table 1 and Figure 1.

Documenting diagenetic features and constraining their formation have been a focus of MSL in its years of study on Mars, with evidence for multiple, overlapping diagenetic events coming in many forms. CheMin X-ray diffraction analyses of rock targets in Yellowknife Bay, Pahrump Hills, Oudam, Hartmann's and Valley/Karasburg/Sutton Island, as well as observations of Ca-sulfate veins, revealed mineral assemblages that were interpreted to be consistent with at least five different diagenetic fluid events (Achilles et al., 2020). Spectral and landscape level textural evidence combined were also interpreted to show that the erosion-resistant VRR was a feature created through late-stage diagenesis (Bennett et al., 2021; Fraeman et al., 2020; Horgan et al., 2020). In situ age dating of jarosite also demonstrates that at least one episode of diagenesis occurred far after the deposition of Mt Sharp, with some phases created squarely in the Amazonian, far more recently than Gale's lacustrine activity in the middle Hesperian (Martin et al., 2017).

Curiosity has also observed significant evidence of late-stage diagenesis in the form of veins, concretions and nodules, and alteration halos all along the rover's traverse (Bennett et al., 2021; David et al., 2020; Frydenvang et al., 2017; Gasda et al., 2022; Horgan et al., 2020; Kronyak et al., 2019; Nachon et al., 2014, 2017; Rudolph et al., 2022; Seeger & Grotzinger, 2024; Stack et al., 2014; Sun et al., 2019; Yingst et al., 2023). These observations indicate that significant groundwater activity persisted even after the disappearance of surface water. Before Curiosity even reached Mount Sharp, diagenetic features were first identified and studied in the mudstone of the Sheepbed member of Yellowknife Bay between sols 126 and 303 (Stack et al., 2014). At the base of Mount Sharp in the Pahrump Hills area, lenticular crystals provided early evidence for gypsum precipitation and are inferred to have formed via diagenetic alterations of that sulfate (Kah et al., 2018). Continuing upwards, Sun et al. (2019) comprehensively characterized the morphology, chemistry, and stratigraphic distribution of diagenetic features across the first ∼300 m of elevation of Mount Sharp and classified them as veins and lamination enhancing textures, as well as four distinct morphological groups of diagenetic nodules: dendrites, spherules, irregular, and flat. Each were postulated to be representative of different formation conditions, with at least six distinct post-depositional aqueous events thought to have occurred in Gale Crater.

Next, Curiosity traversed through this study's regions of interest, VRR and Glen Torridon (Table 1). These two regions are notable for their unique morphologic expressions, stratigraphic interfingering and mineralogic differences (Bennett et al., 2022; Bristow et al., 2021; Fedo et al., 2018). The *VRR* is an erosionally resistant geologic feature that is distinct from orbit both because of its raised topography and strong hematite spectral signature in Compact Reconnaissance Imaging Spectrometer for Mars data (Anderson & Bell, 2010; Fraeman et al., 2016). It spans parts of the Pettegrove Point and Jura stratigraphic members of the Murray formation (Edgar et al., 2020). *Pettegrove Point* is fine-grained and composed of finely laminated mudstone to fine sandstone (Fraeman et al., 2020). *Jura* is also fine-grained, composed of finely laminated mudstone to fine sandstone but with strata meters to decimeters in scale dipping in multiple directions (Fraeman et al., 2020). Vera Rubin ridge has been demonstrated to show evidence of extensive diagenetic modification by multiple fluid events (Achilles et al., 2020; Bennett et al., 2021; Edgar et al., 2020; Fraeman et al., 2020) with mineralogical evidence for acidic, saline fluids (Rampe et al., 2020). These events diagenetically altered the mudstones and horizontal dips, resulting

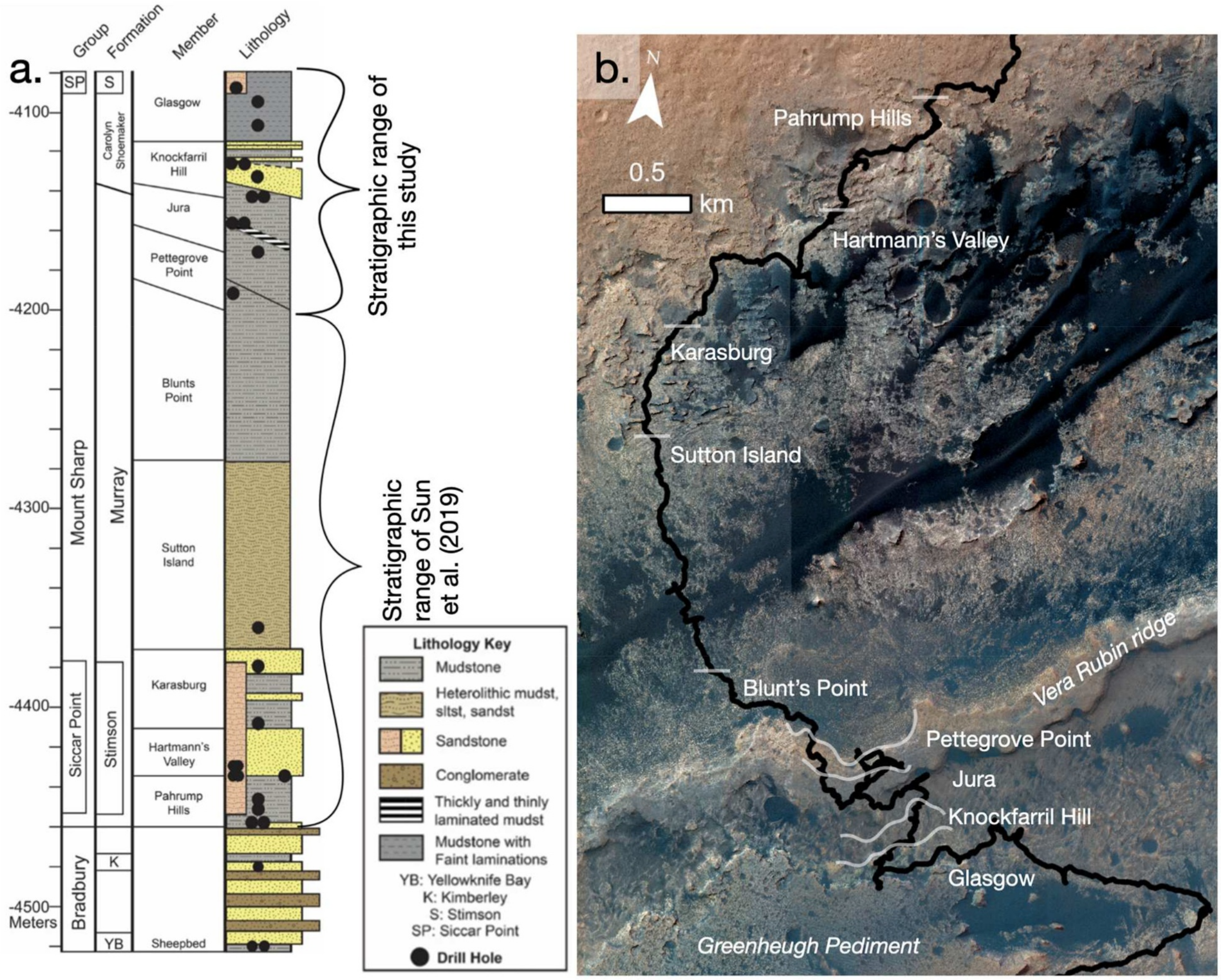

Figure 1. (a) MSL–team schematic stratigraphic column summarizing the geologic units encountered over a lateral traverse into a representative section, with stratigraphic ranges examined in this paper and in Sun et al. (2019) highlighted. (b) Orbital view of relevant member boundaries (gray) along the rover traverse (black), with two major geological features noted in italics.

in its erosional resistance and strong hematite signature from the orbit (Edgar et al., 2020; Fedo et al., 2018; Fraeman et al., 2020). Differing grain sizes of hematite support multiple diagenetic events with early oxidizing fluids near the surface resulting in finer, redder hematite; and later burial resulting in coarser, gray hematite (Bennett et al., 2021; Horgan et al., 2020).

The base of the stratigraphic sequence in Glen Torridon is stratigraphically equivalent to strata outcropping in VRR. *Glen Torridon* is a trough-like geologic feature that spans the upper Jura member of the Murray formation, and the entirety of Knockfarril Hill and Glasgow members of the Carolyn Shoemaker formation. Knockfarril Hill

Table 1
Stratigraphic Units Discussed Here With Their Sol and Elevation Ranges (From Edgar et al., 2020; Fedo et al., 2022; Gwizd et al., 2022)

Formation	Member	Geologic feature	Sol range	Approximate stratigraphic range (m)
Murray	Pettegrove Point	Vera Rubin ridge	1810–1873, 2000–2014, 2024–2045, 2095–2157	−4210 to −4172
Murray	Jura	Vera Rubin ridge and Glen Torridon	1874–1999, 2015–2023, 2158–2439, 2448–2453	−4172 to −4143
Carolyn Shoemaker	Knockfarril Hill	Glen Torridon	2440–2447, 2454–2606, 2817–2950	−4143 to −4117
Carolyn Shoemaker	Glasgow	Glen Torridon	2607–2695, 2735–2816	−4117 to −4072
Stimson	N/A	Greenheugh Pediment	2695–2732	−4050 to −3900

is composed of cross-bedded sandstones while Glasgow is made up of diagenetically overprinted laminated mudstones (Bennett et al., 2022; Caravaca et al., 2022; Fedo et al., 2022; Meyer et al., 2024). Gasda et al. (2022) showed that the different morphologies and chemistries of diagenetic features in Glen Torridon would have to have formed under different environmental conditions, further supporting multiple episodes of diagenetic fluids. VRR and Glen Torridon were originally identified from orbit as spectrally distinct, with the former being dominated by spectral absorptions attributed to hematite, and the latter being dominated by spectral absorptions attributed to clay minerals (Fraeman et al., 2013; Milliken et al., 2010; Sheppard et al., 2021). It is postulated that events in VRR may have simultaneously destroyed its clay minerals, in addition to creating its distinctive hematite (Bristow et al., 2021).

The *Greenheugh pediment* comprises a broad gently sloping wind-etched landform that marks the southern boundary of Glen Torridon. The pediment surface consists of an erosional unconformity, known as the basal *Siccar Point group (SPg) unconformity*, which crosscuts the Mount Sharp group stratigraphy. The unconformity (pediment surface) formed through aeolian erosion and is now capped by the Stimson formation (Banham et al., 2022; Bryk et al., 2025; Watkins et al., 2022). Areas of the Greenheugh pediment that the rover has explored were made up of basaltic eolian sandstones, further indicating a transition from wet to dry environments. Underlying the Greenheugh pediment, the altered upper section of the Glasgow member, known as the Hutton interval, displays light-gray tones and an abundance of nodules and veins (Bennett et al., 2022, Rudolph et al., 2022; Manelski et al., 2023; Seeger & Grotzinger, 2024). This interval is also compositionally distinct, and Thompson et al. (2022), Sutter et al. (2022), and Dehouck et al. (2022) hypothesized this mostly likely reflected subsurface fluids causing concentrated alteration along the SPg unconformity. It is also hypothesized that a diagenetic event along the contact is related to the gray patches of hematite in VRR (Rudolph et al., 2022), as gray hematite signatures were also identified in Glasgow (Rudolph et al., 2022) and is hypothesized to form the alteration of jarosite in sulfide- or chloride-bearing fluids (Knight et al., 2024). Thus, our analysis may help inform this hypothesized relationship as well as constrain the timing and nature of the multiple interactions with groundwater through this region.

2. Methods

2.1. Documentation of Diagenetic Features in MAHLI Images

Data from Curiosity's Mars Hand Lens Imager (MAHLI) were used to classify the types and quantify the size of diagenetic features seen along Curiosity's traverse. MAHLI has a 2-megapixel color camera on Curiosity's robotic arm; it can take focused images with standoffs greater than about 2.1 cm, with a corresponding minimum pixel scale of 14–100 microns per pixel depending on the standoff distance (Edgett et al., 2012). The spatial resolution of MAHLI images makes it an optimal tool for documenting the morphology of late-stage diagenetic features that are millimeters to centimeters in scale.

MAHLI is capable of taking multiple images of a target at different standoffs, each with a different depth of field but the same frame, in order to perform a focus-merge onboard the rover. This creates a single image with a larger depth of field, so that one can survey any part of the image for desirable features, including diagenetic nodules. Our data set consists of all MAHLI focus stack images of rock targets between sols 1900–3049. Images were acquired from the Planetary Science Data System (PDS) and their corresponding label files were automatically downloaded in full-scale JPEG format in Python, with relevant image parameters—pixel scaling, standoff distance, target information—automatically extracted for analysis and used to identify duplicate images. In conjunction with MSL localizations, we used the sol of image acquisition to approximate coordinates and elevations where images were taken.

Once acquired, we examined each image individually to characterize the presence and type of diagenetic features using the classification scheme developed by Sun et al., 2019. We identified flat, irregular, spherule, or dendritic nodules, as well as veins or lamination-enhancing features. We also took note of the texture of irregular nodules as being rough or smooth, and recorded whether a given type of nodule was present or not for each target. We also took note of the dominant nodule type in each image, defined as the nodule morphology that appears most frequently and/or distinctly in an image.

To measure diagenetic nodule sizes, we modified a Python point-picking script (Zucker, 2021) to chronologically read MAHLI images and their pixel scales and allow for measurements on a custom GUI. The tool lets one draw

10.1029/2024JE008891

two lines per measurement on the image, nominally representing the longest dimension of a given nodule, as well as the orthogonal dimension. Multiple measurements can be made on the same image. This allows for measurements of the general size scale of these nodules, as well as an elliptical approximation of the nodule area as seen by MAHLI.

2.2. Documentation of Diagenetic Nodules in Mastcam Images

Data from Curiosity's Mast Camera (Mastcam) were used to survey the presence and density of diagenetic features at the landscape level. Mastcam consists of two cameras with 1600 × 1200 pixel detectors, M34 with an f/8, 34 mm focal length lens, and M-100, with a f/10, 100 mm focal length lens (Malin et al., 2017). It can capture true color images using Bayer filters, and multispectral images with its seven science filters per camera eye (Malin et al., 2017). Mastcam mosaics are useful for identifying the context in which nodule morphologies occur because they survey a much larger field of view (meter-to 10s of meters-scale) than MAHLI images (millimeter-to centimeter-scale).

For this work, we compiled a database of Mastcam Bayer filter color mosaics collected within a few meters of the rover from the Analyst's Notebook in the PDS for all available sols. These mosaics included standard 3 × 2 M34 workspace mosaics that are captured at the end of almost every drive and cover the area immediately in front of Curiosity that is accessible by the rover's arm. These workspace mosaics commonly have high enough spatial resolution to resolve the largest diagenetic features. Moreover, given that MAHLI targets are selected from the same Mastcam workspace mosaics, observations of diagenetic features in MAHLI images are complementary with those made in Mastcam (with the exception of features that are too small to see in the M34 Mastcam mosaics). A select number of other Mastcam mosaics (Figure S1 in Supporting Information S1) were also examined to survey the type and density of late-stage diagenetic features when they were collected close enough to the rover to have resolution that permitted the identification of these features.

Similar to MAHLI observations, we recorded, for each mosaic, the presence of diagenetic nodules and veins. Due to resolution limitations, differences between irregular and smooth nodules could not be reliably distinguished. This process was conducted on an image-by-image basis, meaning that an image was noted as containing a certain type of nodule as long as it was present on one visible area of bedrock in the mosaic. As for MAHLI, we observed the dominant nodule morphology across each mosaic.

In addition, we qualitatively took note of whether nodule-bearing rocks in each Mastcam mosaic contained them at low, medium, or high density. This constituted a similar approach as Sun et al. (2019), where the highest density within a Mastcam mosaic was recorded for that position. Rocks where diagenetic features covered approximately <1%, 1%–30%, and 30+% of the visible rock surface were labeled as low, medium, and high, respectively (Figure S1 in Supporting Information S1).

2.3. Integration in Orbital and Stratigraphic Context

To contextualize nodule findings with orbital data and stratigraphy, QGIS was used to map nodules based on MSL localizations. The Mars MSL Gale Merged Orthophoto Mosaic 25 cm v3 was used as a basemap of the Gale crater (Calef III & Parker, 2016).

Vera Rubin ridge and Glen Torridon were originally defined based on orbital spectra, which identified the former as hematite-rich, and the latter as clay-rich. In situ observations of Gale crater have since revealed that both hematite and clay minerals are present throughout both regions (Vasavada, 2022). This has motivated the definition of more detailed stratigraphic members characterized by their diverse depositional environments. Within the lacustrine Murray formation, the Pettegrove Point member begins with VRR, which bears strong spectral signatures of red crystalline hematite (Fraeman et al., 2016). It is overlaid by the Jura member, which includes part of VRR as well as Glen Torridon, and is defined based on strong smectite signatures (Fedo et al., 2020). Above the Jura member are the Knockfarril Hill and Glasgow members, the first two members within the newly defined Shoemaker formation (Vasavada, 2022). In contrast to the Murray formation's lacustrine origins, Knockfarril Hill is associated with a fluvial or lake-margin depositional environment (Fedo et al., 2022). Glasgow, which overlies Knockfarril Hill, is interpreted to have formed during a later period of lacustrine deposition (Fedo et al., 2022). For elevations and lithology of each member, see Figure 1. We map the locations of concretions against the boundaries of each of these members, in order to contextualize the presence of diagenetic nodular textures with the changes between both stratigraphic members, and the Murray and Shoemaker formations.

2.4. Statistical Analyses

We conducted regression analyses to examine two key relationships: (a) the predictive relationship between in-scene feature density and depth below the pediment, and (b) the correlations between different feature morphologies while controlling for the presence of other features. For the first analysis, we estimated the ordinary least squares (OLS) regression model described by

$$\text{Depth below pediment}_i = \beta_0 + \beta_1 \text{ feature density}_i + \varepsilon_i$$

where β_1 captures the effect of feature density (ρ) on depth. For the second analysis, we estimated the correlations between morphological features in scenes (holding all other features constant) with the following OLS regression model:

$$\text{Morphology}_i = \beta_0 + \Sigma_j \beta_j \text{Morphology}_{i,j} + \varepsilon_i$$

where Morphology$_i$ is a binary variable representing the presence of a specific feature in a scene i, Morphology$_{\mathrm{ij}}$ are binary variables that are 1 if Morphology j is present in scene i and zero otherwise. β_j quantifies the association between each pair of features while controlling for the others. This allows us to determine, for example, whether spherules and veins are less likely to co-occur when accounting for other morphologies. $N = 380$ scenes. All regressions were estimated using the fixest R package with heteroskedasticity-consistent robust standard errors.

3. Results

3.1. Classes of Diagenetic Features

We find that all of the diagenetic nodular features observed in Mastcam images and MAHLI focus-stack images fit well into the classes of spherules, irregular, and flat morphologies first described by Sun et al. (2019) (Figures 2–4). In both the MAHLI focus-stack images and Mastcam image mosaics, we did not observe any new morphologies beyond those observed in Sun et al., 2019. Irregular nodular textures were by far the most common overall, with spherules being the second most common morphology (Figures 3–5).

While previously termed concretions (Sun et al., 2019), we describe these diagenetic features as nodules to be origin agnostic (e.g., Gasda et al., 2022). We noted the following characteristics about each morphology, which helped us to identify them based on previous work, presented here with characteristic visual examples (Figure 2). Their distribution within the strata of Mount Sharp can be seen in Figures 3 and 4.

3.1.1. Spherules

Spherules are spherical or near spherical in shape with surfaces ranging from smooth to rough in texture (Figure 2a). Color of spherules varies from host rock color to reddish-brown to dark gray.

3.1.2. Irregular Concretions

Irregular concretions are similar to spherules in color but have shapes that vary between larger rough lumps, smoother bumps, and extended teardrop shapes (Figures 2b and 2c). Irregular concretions comprise the most diverse group, as it often encompasses those that are distinctly concretions but not distinct enough to form their own classification. Spherules and irregular concretions often appear together, and the boundary between the two is sometimes difficult to distinguish.

3.1.3. Dendrites

Dendrites, as seen in Sun et al. (2019), are nodular textures which distinctly branch out from a single point. We did not observe any equivalent nodules.

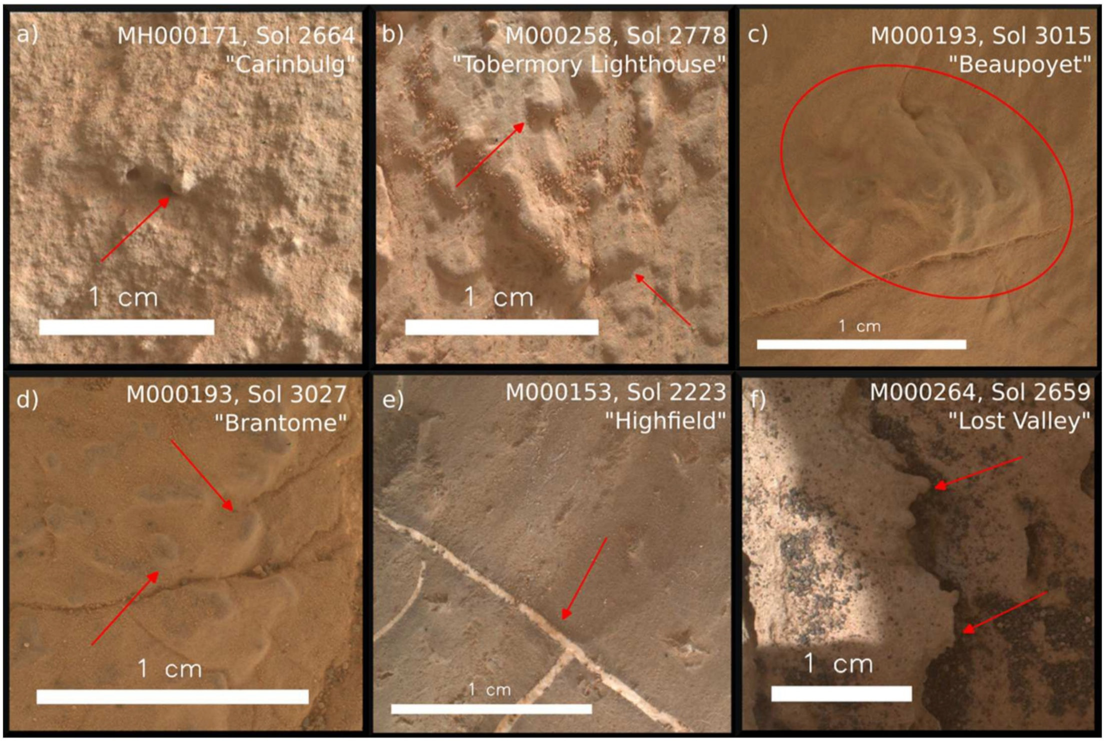

Figure 2. Examples of Mars Hand Lens Imager (MAHLI) diagenetic feature/nodular texture morphologies with corresponding scale bars, locations, and image identification. Each of these morphological classes was first identified by Sun et al. (2019), and their observations provided a framework for making these identifications. The morphology classifications are as follows: (a) spherule, (b) irregular (smooth), (c) irregular (rough), (d) flat, (e) veins, (f) lamination-enhancing features.

3.1.4. Flat Nodules

Flat nodules appear to be generally found on top of flatter sections of bedrock but are distinct in color from their host bedrock (Figure 2d). As the name describes, they are morphologically fairly flat and protrude very little from their host rock compared to other types of concretions. They range in color from brown to black.

3.1.5. Veins

Veins are usually light-toned with occasional appearance of dark-toned veins. As noted in Sun et al. (2019), they are one of the most prevalent types of diagenetic features in Mount Sharp and sometimes crosscut other features (Figure 2e).

3.1.6. Lamination-Enhancing Features

While not a distinct nodular morphology, lamination enhancing features are host-colored features that are resistant to erosion and help to accentuate the visible lamination of the bedrock (Figure 2f).

3.2. Distribution and Density of Diagenetic Features

We also observe that the density of diagenetic features at a locality is variable along the traverse with the densest concentrations of features located near Curiosity's dip into the Greenheugh pediment (Figure 6). Most notably, there is a complete absence of all diagenetic features we classified except for veins for most of the Knockfarril Hill member in both Mastcam and MAHLI images (Figures 3 and 6).

For most of the traverse examined here, the dominant nodular texture type is either spherule or irregular (Figure 5). Each nodular type is usually dominant for a series of observations in both Mastcam and MAHLI. Most irregular nodules observed were smooth in texture (Figure 7b). There is no strong trend dictating where rough irregular textures are found; instead, they are found intermittently wherever nodules are observed.

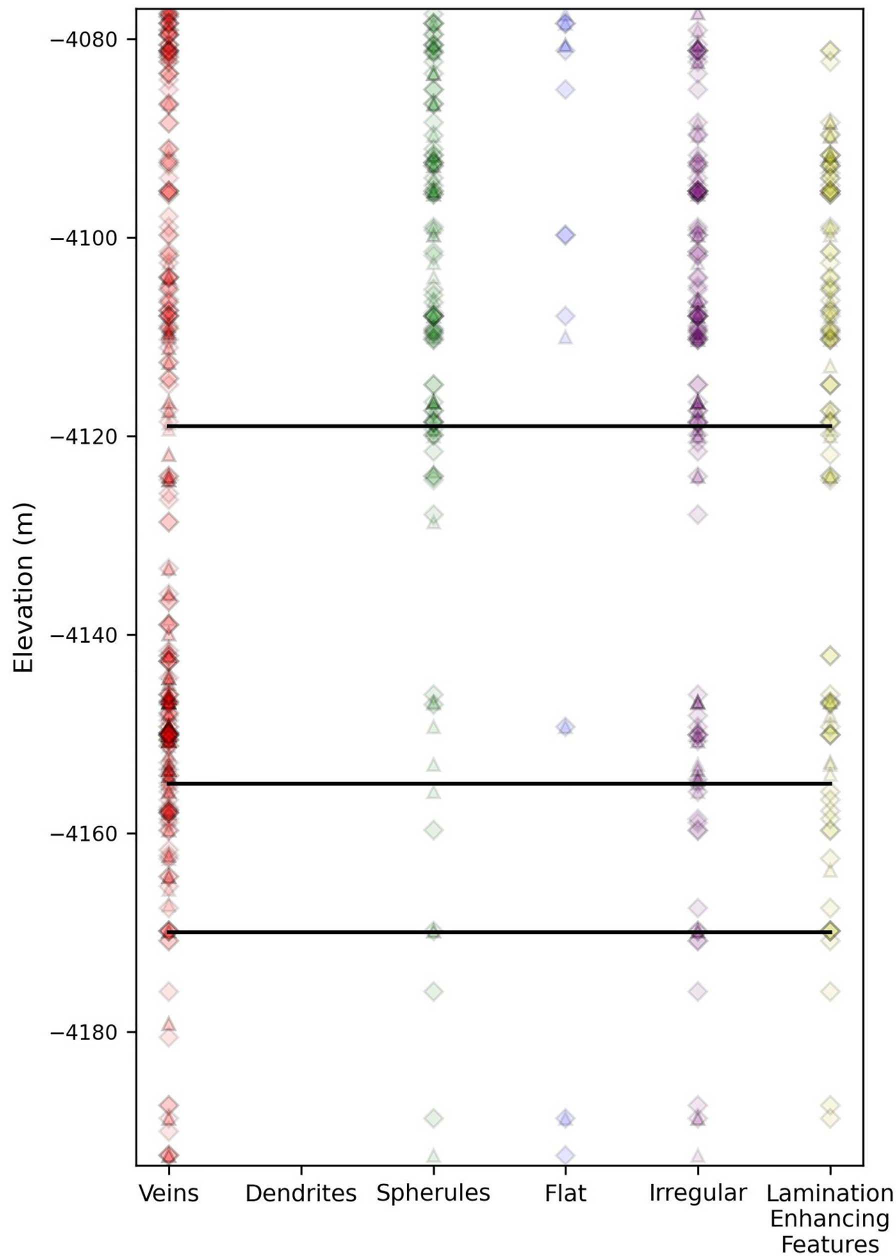

Figure 3. Diagenetic features versus elevation for sol ranges covered in this paper. Stratigraphic member boundaries are indicated as horizontal lines, and member names are written on the right. Detailed description of the characteristics of each stratigraphic member can be found in Fedo et al., 2022. Triangular markers correspond to our MAHLI observations and diamond markers correspond to Mastcam mosaic observations.

We found that spherules and irregular nodular textures often, but not always, are found in the same regions (Figure 7). The main place where spherules are less abundant than irregular is in the transitional region from Jura to Knockfarril Hill (Figure 5). This may be due to the fact that these classes of nodular textures are more similar than any other two classes. While rough irregular nodular textures look distinct from spherules, some smooth irregular nodular textures can look like drawn out spherules but retain similar colors. Consequently, they can be difficult to distinguish between, especially in broader Mastcam images where finer details are challenging to resolve.

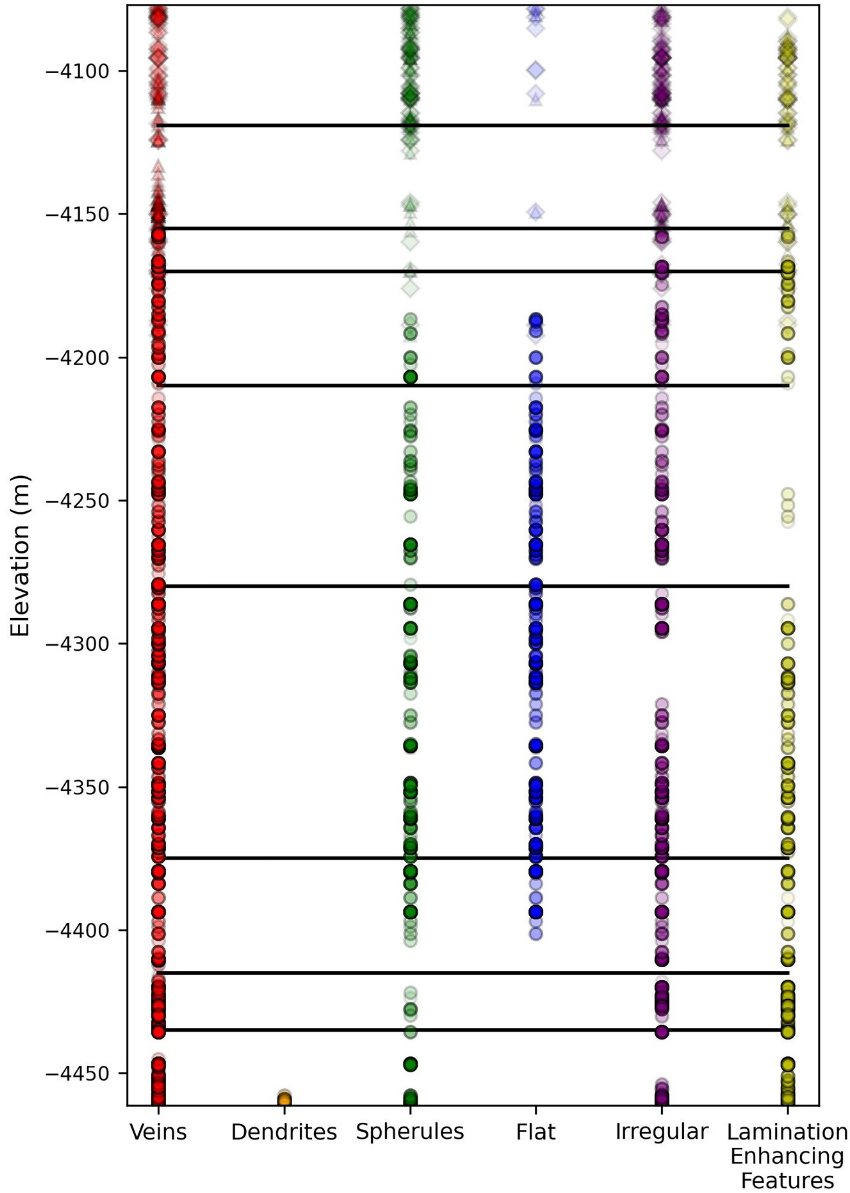

Figure 4. Diagenetic features versus elevation from this work and Sun et al. (2019). Individual columns are sorted by diagenetic feature morphology and divided by stratigraphic member boundaries. Stratigraphic member boundaries are indicated as horizontal lines, and member names are written on the right. Detailed description of the characteristics of each stratigraphic member can be found in Fedo et al., 2022. Triangular markers correspond to our MAHLI observations, diamond markers correspond to Mastcam mosaic observations, and circular markers correspond to observations made by Sun et al. (2019) using either instrument.

On the other hand, flat nodular textures are significantly less common throughout most of Glen Torridon than was previously observed (Figures 4 and 7). Dark and flat nodular textures most closely resembling those seen in Sun et al. (2019) were only consistently observed over the period of sols 3027–3036, while redder or lighter flatter nodular textures were only observed twice in the VRR. However, where flat nodular textures are found within the clay sulfate transition, they are the dominant morphology and found in very high density (Figures 5 and 6).

Throughout the portion of the traverse examined here, veins were observed consistently regardless of nodular texture presence. Lamination enhancing features are also found in most places where nodular textures are also observed with high frequency. They are common in the high-density region near Curiosity's entrance into the

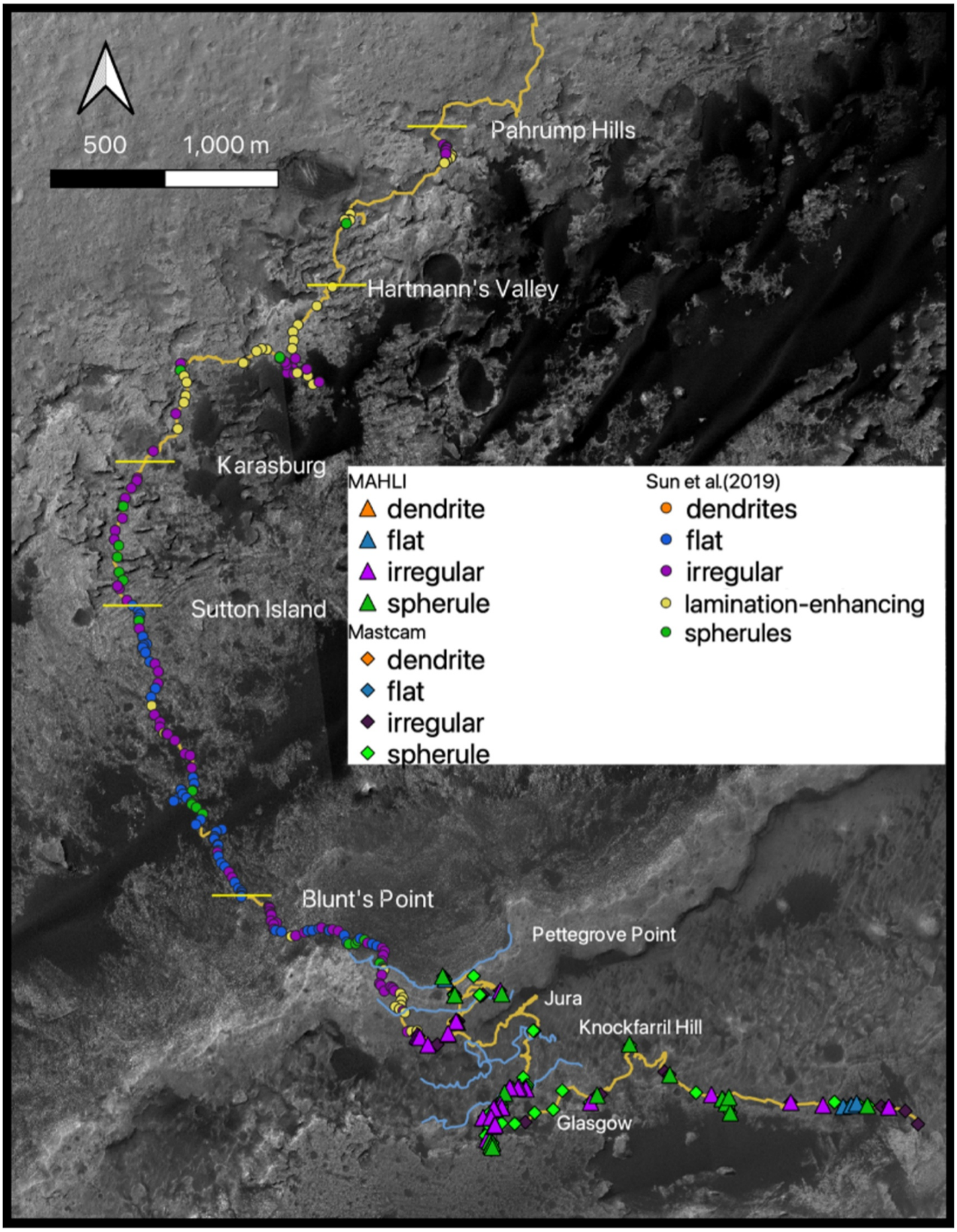

Figure 5. Map showing dominant diagenetic nodular textures on Mount Sharp as recorded by Sun et al. (2019) and this study. Circular markers are used for nodules observed in Sun et al. (2019), while diamond and triangular markers represent Mastcam and MAHLI, respectively, in this study.

Greenheugh pediment (Figures 6 and 7). However, lamination enhancing features are very rare in the clay-sulfate transition, with only one observation made. This contrasts with the high density of nodular textures in that region.

We find that qualitative nodule density is generally significantly lower than that observed pre-sol 1900. In VRR, distinct nodular textures are not observed at many points; when seen, they are generally in low to medium density (Figure 6) with the exception of two locations where spherules are observed (Figure 7a). The Greenheugh

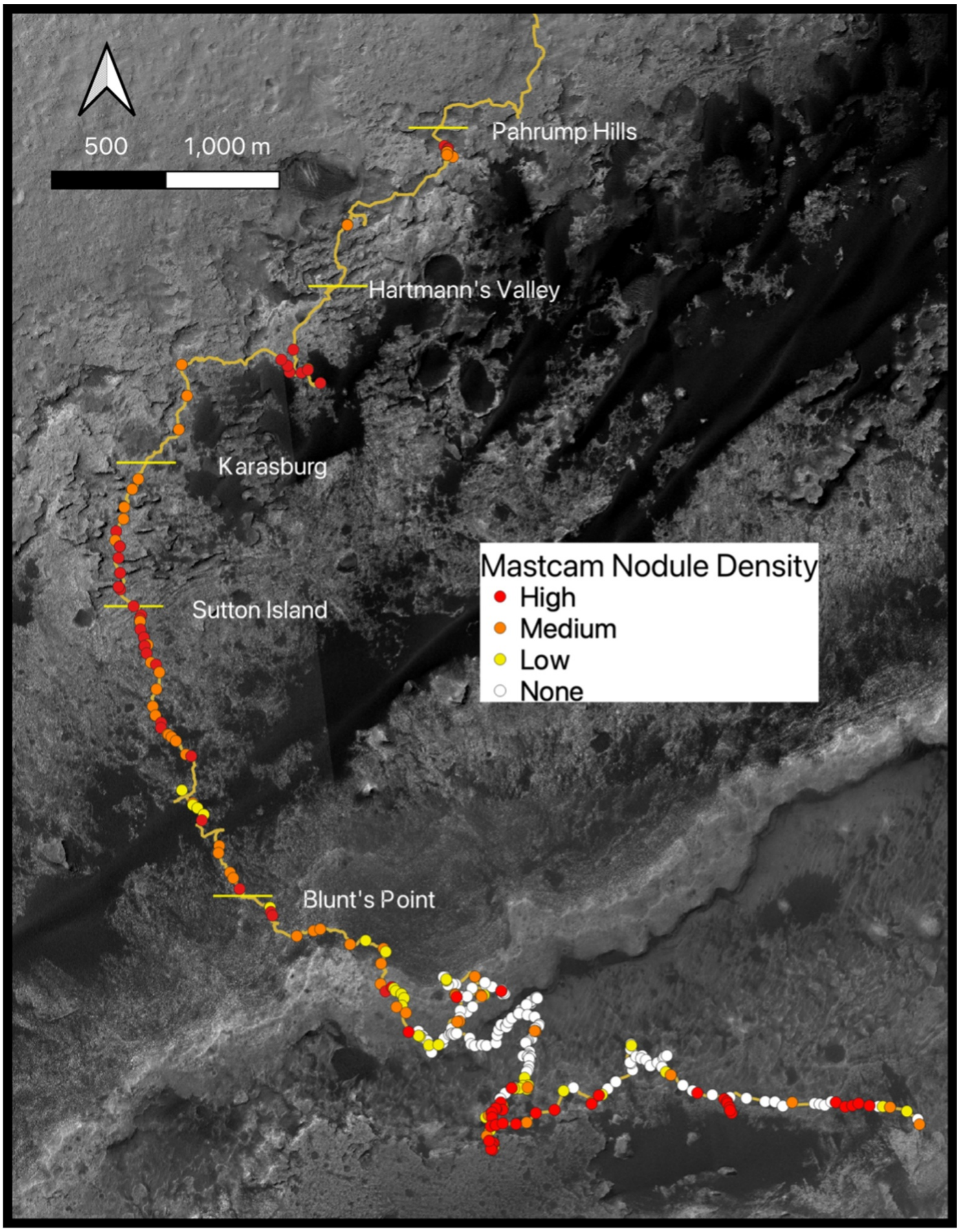

Figure 6. Map showing nodule density concentration as qualitatively determined by examination of MAHLI images and Mastcam workspace mosaics.

pediment and the clay-sulfate transition both have a high density of nodular textures. These regions of high nodule density are separated by stretches with low to zero nodule density. This is a strong contrast to observations from approximately Sols 1417–1900, where nodules are observed in a continuous stretch with mostly medium to high density.

3.3. Size of Diagenetic Nodular Textures

Measurements of the nodules found them to range from mm-to cm-scale in size. The estimated elliptical area of the nodules ranged from 0.8 to 49.3 mm^2, while the longest dimension of the nodules ranged from 0.562 to 4.739 mm (Figure 8). The smallest nodules observed within both VRR Glen Torridon were similar in size to those previously observed on lower Mount Sharp (Sun et al., 2019). However, with a few exceptions on the boundary

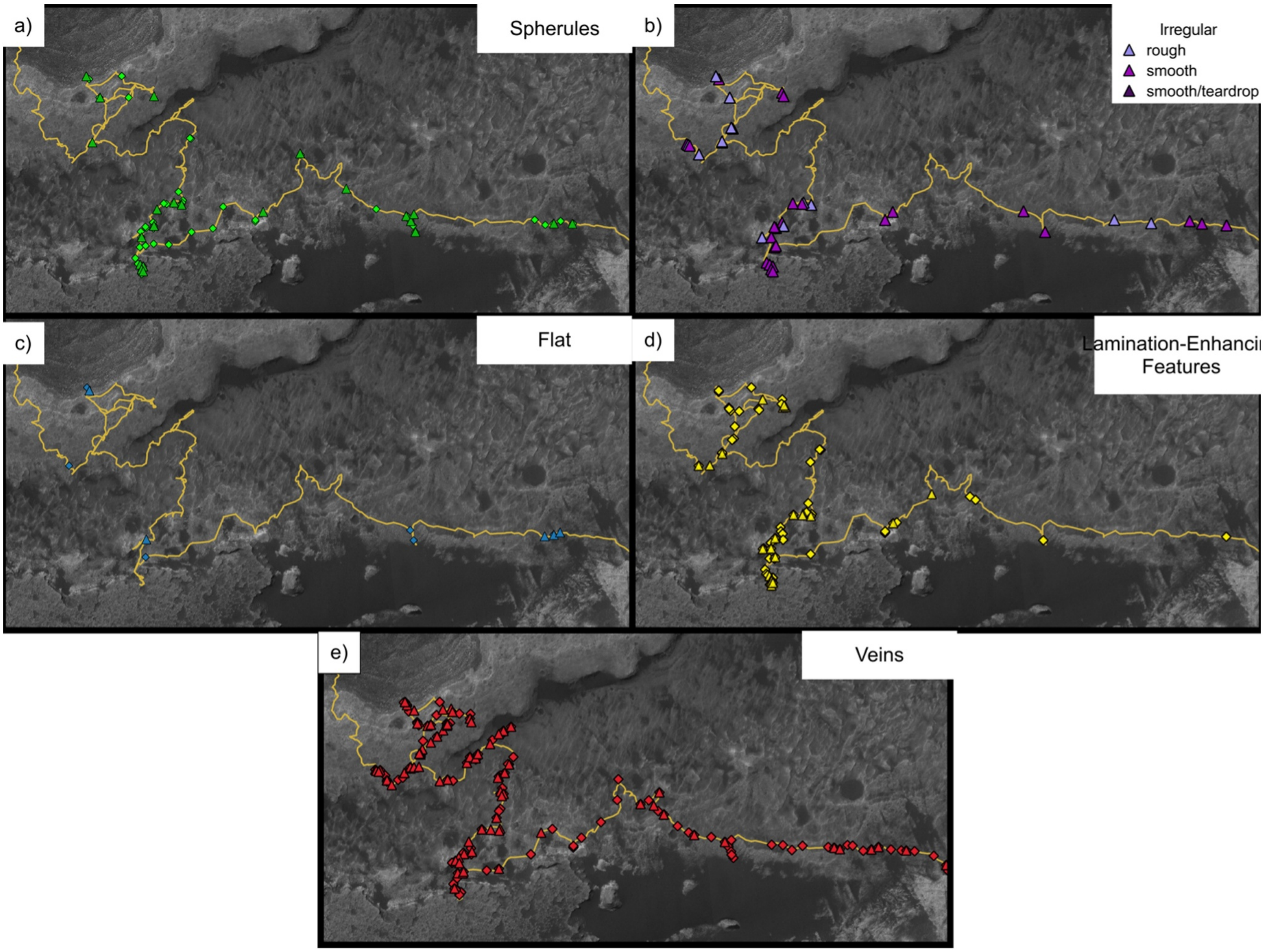

Figure 7. Location and concentration of each diagenetic feature by morphology, as observed by both Mastcam and MAHLI, Sols 1900–2049. Features in each map are (a) spherules (b) irregular, including nodule texture sub-type (c) flat (e) lamination-enhancing features and (f) veins. Triangular markers denote MAHLI observations, whereas diamond-shaped markers denote observations in Mastcam mosaic images.

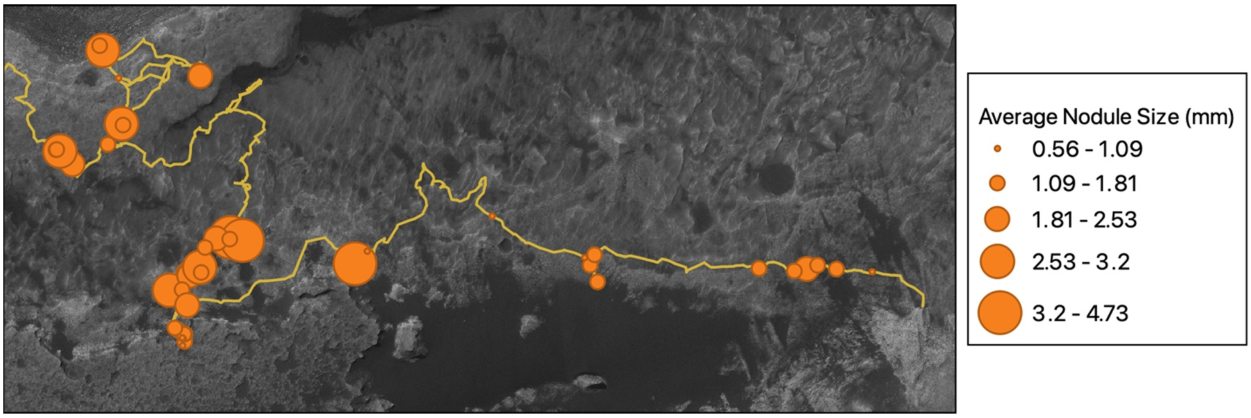

Figure 8. Map of the length of observed diagenetic nodules in the newly observed region. The size of each marker scales with the average "long-axis" length (the length of the longest observed dimension for any given nodule) of the nodular textures at a given location, while observations with no nodular textures have been omitted.

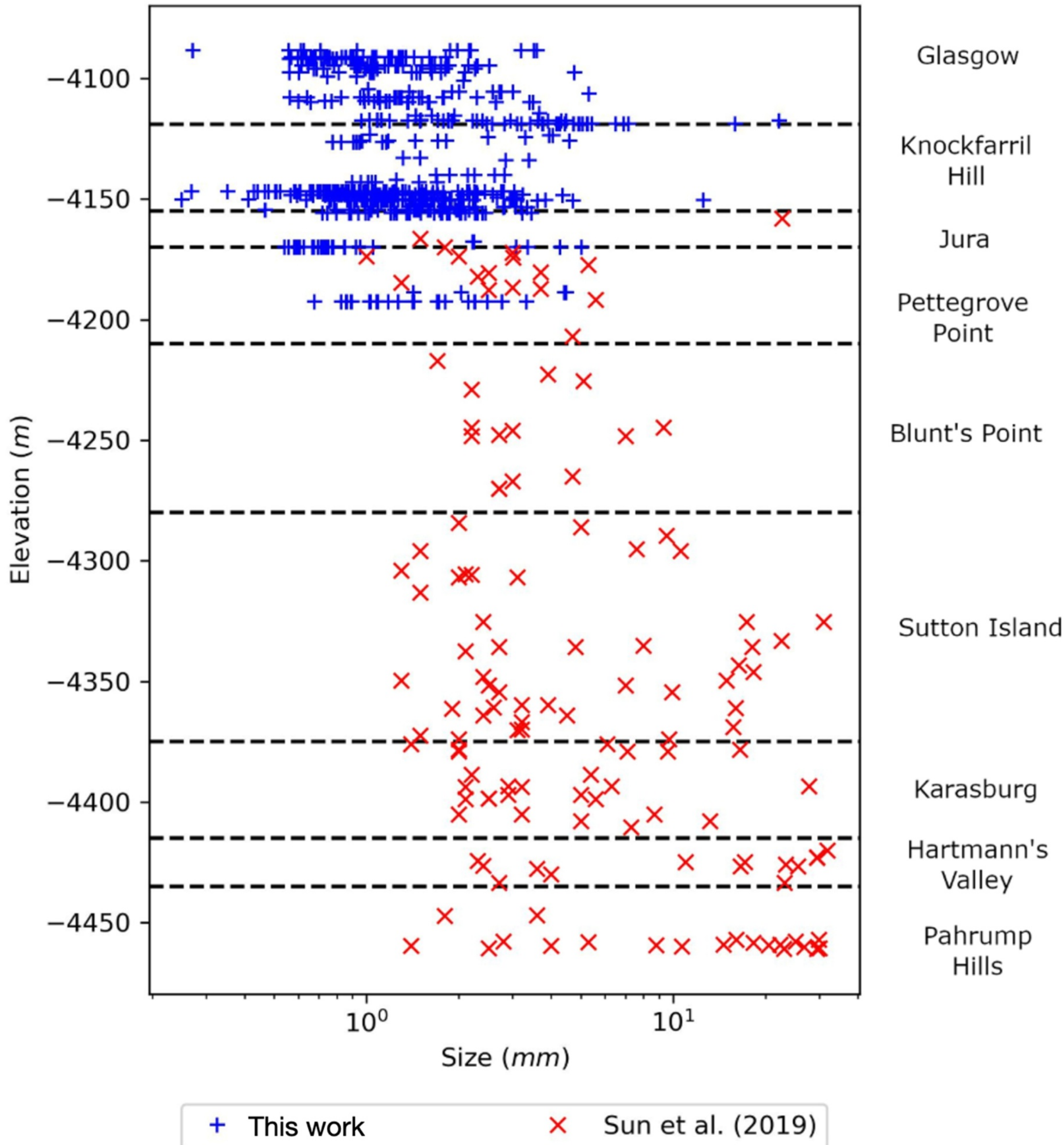

Figure 9. Nodule size versus elevation and approximate stratigraphic member, including data from Sun et al. (2019) measuring nodular textures on lower Mount Sharp. Nodules measured were chosen as representative of their respective images, including measurements of average, largest and smallest nodules in a given scene.

between Glasgow and Knockfarril Hill, the largest nodules frequently observed were five to six times smaller than the largest nodules *previously* observed through Sutton Island (Figure 9). When combined with data from lower Mount Sharp, it can be seen that the trend of decreasing nodular size with elevation, noted in Sun et al., 2019, continues into this newly mapped region (Figure 9).

3.4. Examples of Targets With Multiple Classes of Diagenetic Features

While most scenes that contain diagenetic nodular textures have a single dominant morphology present, some contain multiple morphologies in the same scene. The two most common types, spherules and irregular nodules, often exist together (Figures 3 and 7). Flat textures were observed later in Curiosity's traverse (sols 3027–3035) as

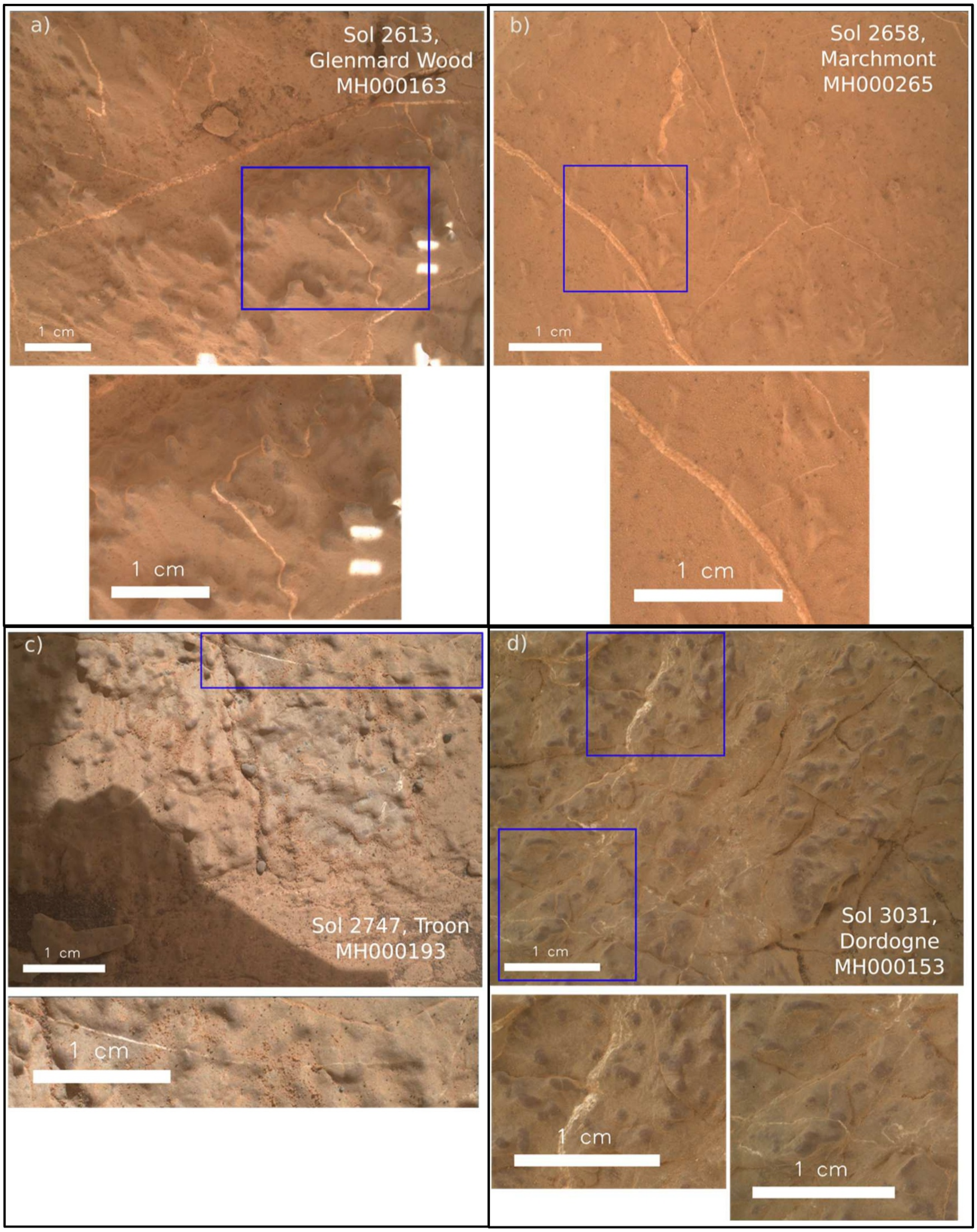

Figure 10. MAHLI images showing veins that overlie, crosscut, or have their paths influenced by the presence of diagenetic nodules, taken from throughout the stratigraphic range examined. (a) Glenmard Wood, Sol 2613, featuring veins wrapping around irregular nodules. (b) Marchmont, Sol 2658, featuring veins overlying irregular nodules. (c) Troon, Sol 2747, featuring veins cutting through spherule and irregular nodules. (d) Dordogne, Sol 3031, featuring veins crosscutting flat nodular textures.

a dominant texture, accompanying some features that were somewhat ambiguous in morphology but looked close to spherules in nature.

Additionally, veins–which were observed both alongside and without diagenetic nodular textures–were observed overlying or cutting through nodules of multiple morphologies (Figure 10).

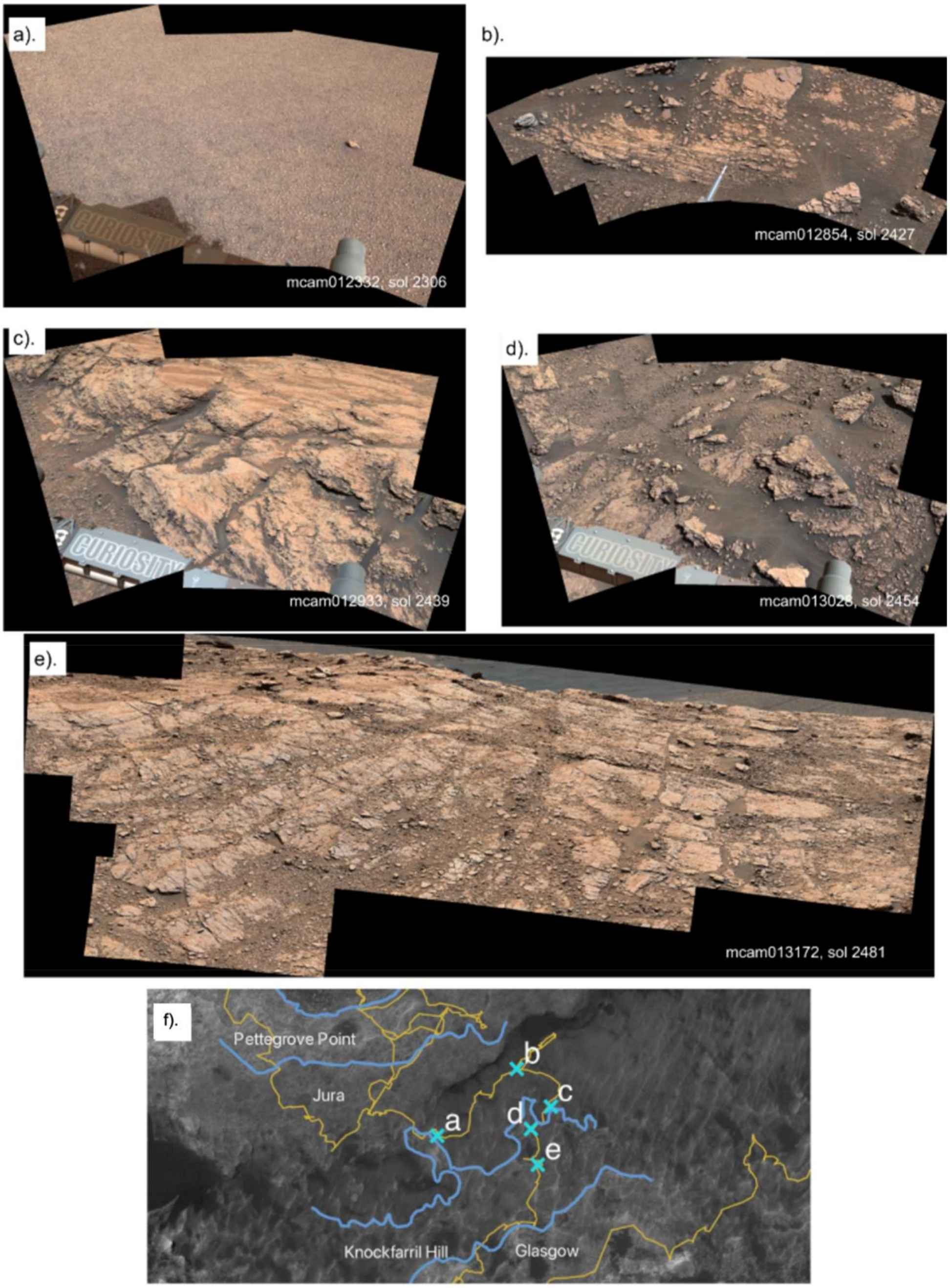

Figure 11. (a)–(f) Examples of Mastcam workspace mosaics where diagenetic nodular textures are absent from sols 2306–2481, primarily located in the Jura and Knockfarril Hill members, and ordered chronologically. (a)–(c) Are located in the Jura member, while (d)–(e) are located in Knockfarril Hill (f) Map of locations of subfigures (a)–(e), with member boundaries in blue and Curiosity's traverse in yellow. (a) mcam012332, sol 2306, (b) mcam012854, sol2427, (c) mcam012933, sol 2439, (d) mcam013028, sol 2454, (e) Glen Etive drill site, mcam013172, sol 2481. Image credit: NASA/JPL-Caltech/MSSS.

3.5. Examples of Targets Lacking Diagenetic Features

Diagenetic nodular textures are notably absent in the MAHLI data set from elevation −4143.8 to −4117.47 m (sols 2258–2574) and from elevation −4146.92 to −4124.1 m (sols 2246–2446, 2459–2565) in Mastcam mosaics (Figure 11). This elevation range primarily encompasses much of the Jura and Knockfarril Hill members within the clay-rich Glen Torridon region, where reduced diagenesis had been previously observed (Gasda et al., 2021). It is important to note that the lack of diagenetic nodules throughout most of Knockfarril Hill is not due to a

Table 2
Feature Density Predicting Depth Below the Pediment

Dependent variable:	Depth below pediment
Model:	(1)
Variables	
Low density in scene	−7.492***
	(1.424)
Medium density in scene	−2.861
	(2.368)
High density in scene	8.787***
	(2.036)
Fit statistics	
Observations	856
R^2	0.04423

Note. Heteroskedasticity-robust standard-errors in parentheses Signif. Codes: ***: 0.001, **: 0.01, *: 0.05.

complete lack of available bedrock to observe, although this was the case in some areas. Bedrock throughout Glen Torridon was seen to have plentiful visible primary laminations of its sedimentary layers, as well as veins, providing evidence of some diagenetic activity. Slightly increased numbers of observations of diagenetic features in the Mastcam mosaics can likely be attributed to the much wider field of view of that instrument compared to MAHLI, making it better at representatively sampling a given location.

3.6. Statistical Analysis

3.6.1. Feature Density and Depth Below Pediment

The relationship between feature density within the scene and the depth below the pediment is shown in Table 2 and Figure S2 in Supporting Information S1. Low feature density is significantly ($p < 0.01$) negatively correlated with depth below the pediment; medium feature density is not correlated with depth below the pediment; and high feature density is significantly ($p < 0.01$) positively correlated with depth below the pediment, with the highest density of features immediately below the pediment and decreasing away from it. The largest features are all clustered in the 10–15 m below the pediment bin.

The relationships between the different feature morphologies are shown in Table 3. Veins were significantly ($p < 0.001$) negatively correlated with spherules and flat nodules, and significantly ($p < 0.001$) positively correlated with irregular nodules.

3.6.2. Feature Size and Abundance versus Elevation and Depth Below Pediment

The relationship between feature count and size sorted by elevation is shown in the histogram and box-and-whisker plots in Figure 12. The relationship between feature count and size sorted by depth below the Greenheugh pediment is shown in Figure 13.

Table 3
Correlation Between Feature Morphologies

Dependent variable:	Veins	Spherules	Flat	Irregular	Lamination en.
Model:	(1)	(2)	(3)	(4)	(5)
Variables					
Spherules	−0.4327***		−0.0413	−0.0649**	−0.0937
	(0.0659)		(0.0275)	(0.0237)	(0.0566)
Flat	−0.4742***	−0.9851***		−0.8730***	−0.1287
	(0.0704)	(0.0148)		(0.0240)	(0.0673)
Irregular	0.1880***	−0.0658*	−0.0371		0.0413
	(0.0364)	(0.0265)	(0.0249)		(0.0345)
Lamination-enhancing	−0.0344	−0.1478	−0.0085	0.0643	
	(0.0932)	(0.0886)	(0.0071)	(0.0516)	
Veins		−0.3050***	−0.0140	0.1307***	−0.0154
		(0.0524)	(0.0096)	(0.0258)	(0.0416)
Fit statistics					
Observations	380	380	380	380	380
R^2	0.16725	0.18213	0.07086	0.07570	0.01894

Note. This is controlling for the presence of other features. For example, cell (1,1) is where spherules are observed, we are less likely to observe veins, controlling for all other features. Heteroskedasticity-robust standard-errors in parentheses Signif. Codes: ***: 0.001, **: 0.01, *: 0.05.

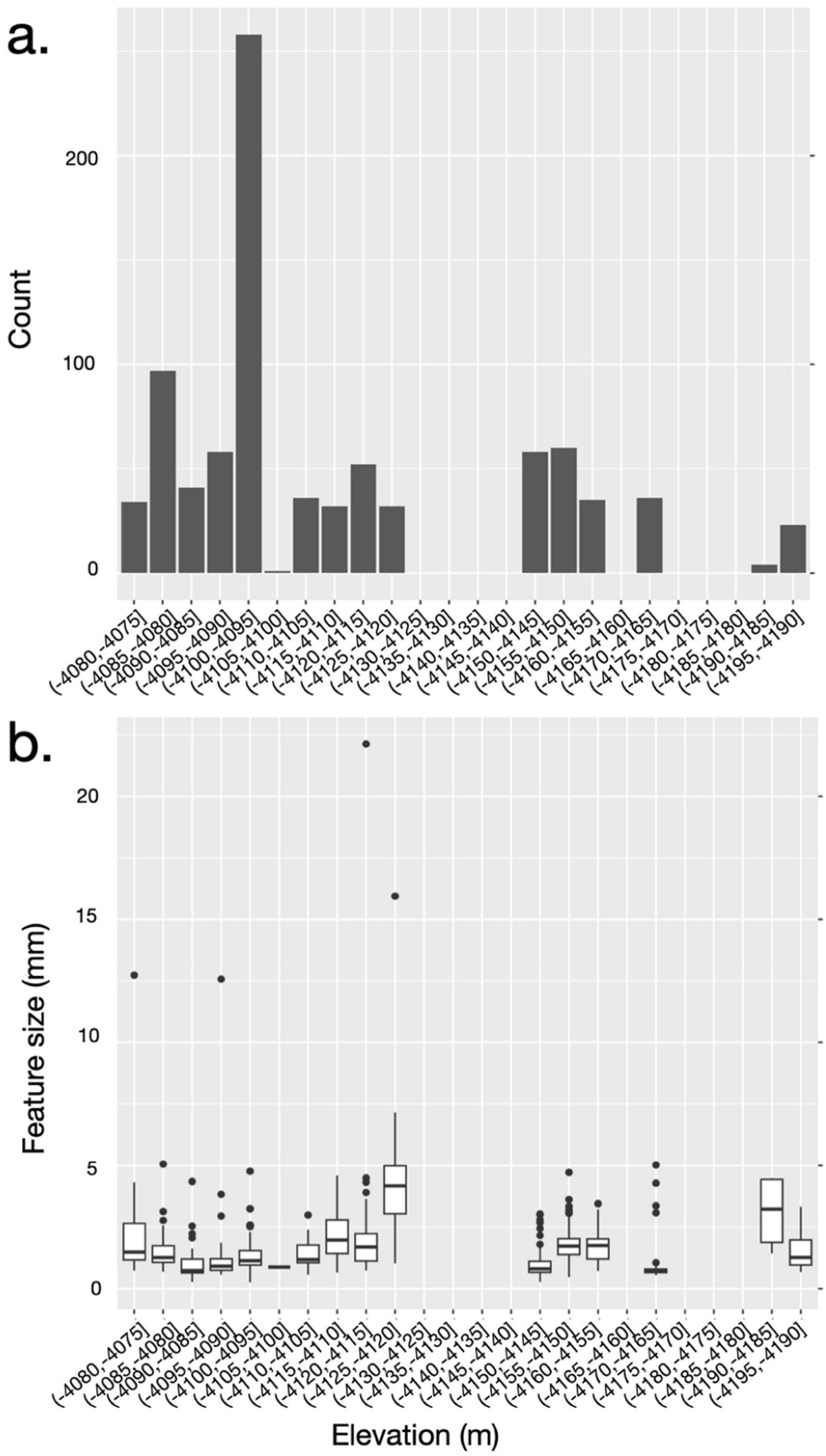

Figure 12. The count and size of features sorted by elevation (m) from −4075 to −4195 m. Bin size of 5 m. (a) Counts of all features in each elevation bin. (b) Box and whisker plots showing mean, standard deviation, and outliers in each elevation bin.

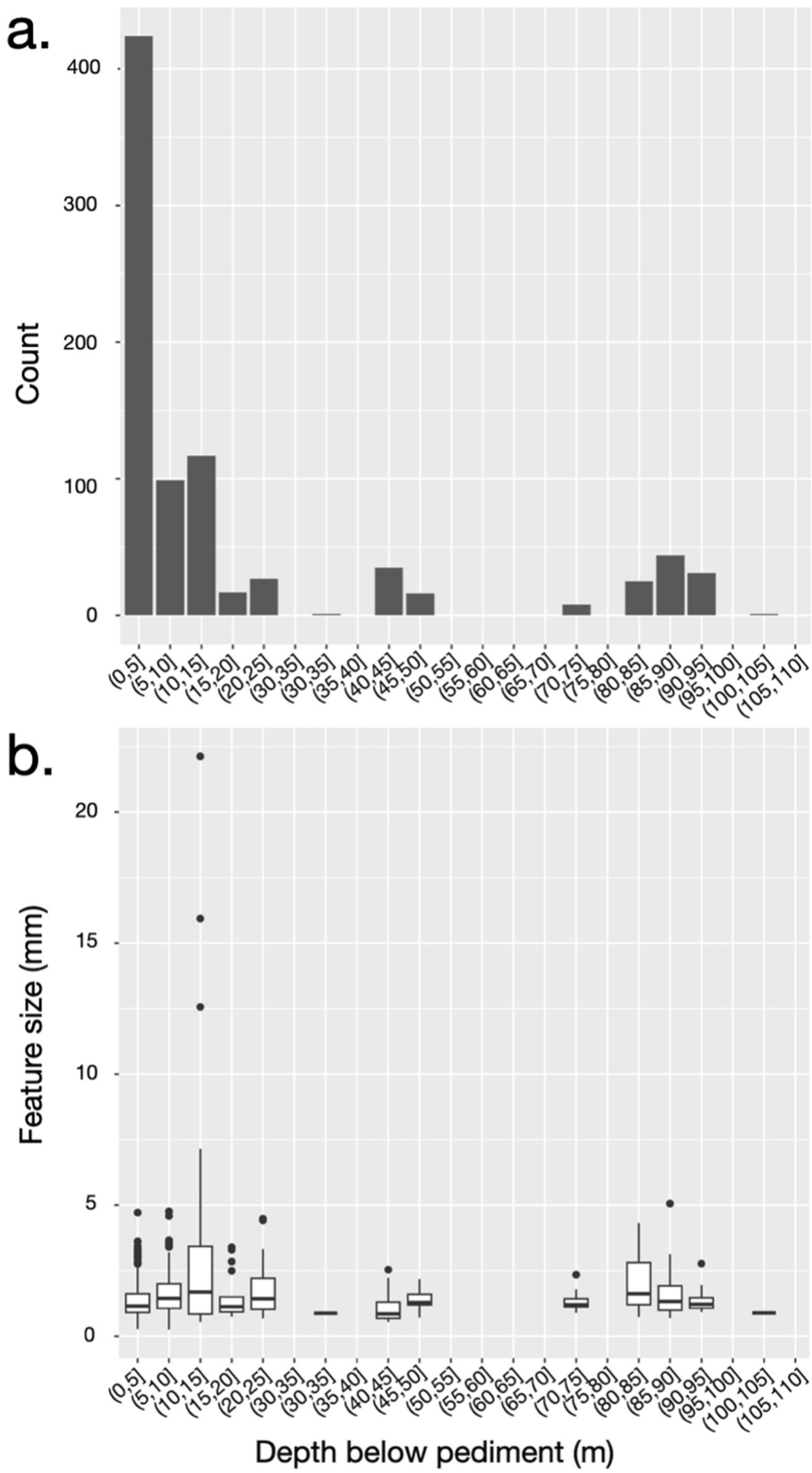

Figure 13. The count and size of features sorted by depth below the pediment (m) from 0 to 110 m. Bin size of 5 m. (a) Counts of all features in each elevation bin. (b) Box and whisker plots showing mean, standard deviation, and outliers in each elevation bin.

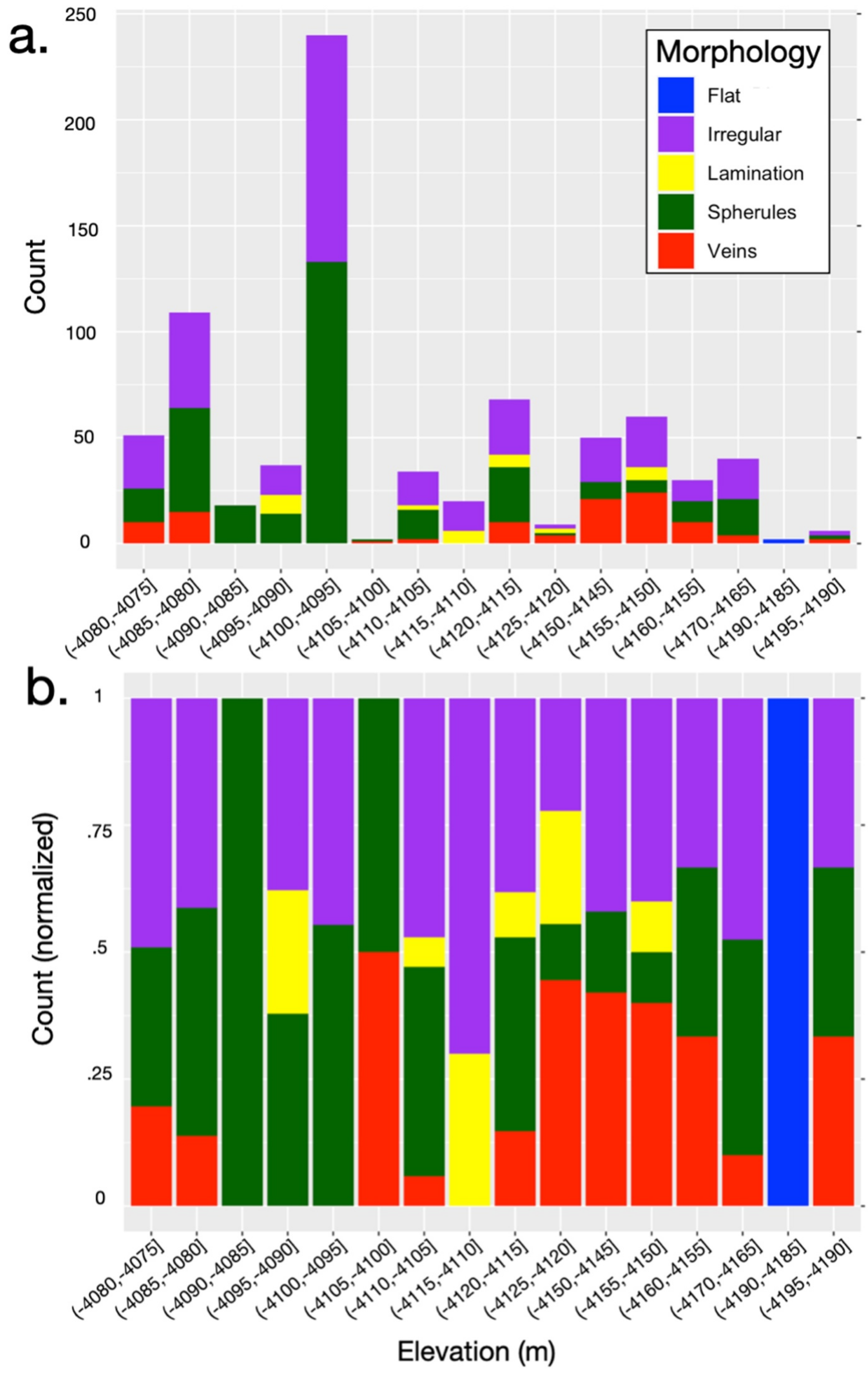

Figure 14. The count of features sorted by elevation (m) from −4075 to −4190 m. Bin size of 5 m. Note that elevation ranges with no features are omitted. (a) Total counts within that elevation range. (b) Normalized counts in that elevation range to highlight changes in proportions of different morphologies.

3.6.3. The Relationship Between Elevation, Depth Below Pediment, and Feature Type

The relationship between feature count and morphology sorted by elevation is shown by the histogram in Figure 14. The relationship between feature count and morphology sorted by depth below the Greenheugh pediment is shown in Figure 15.

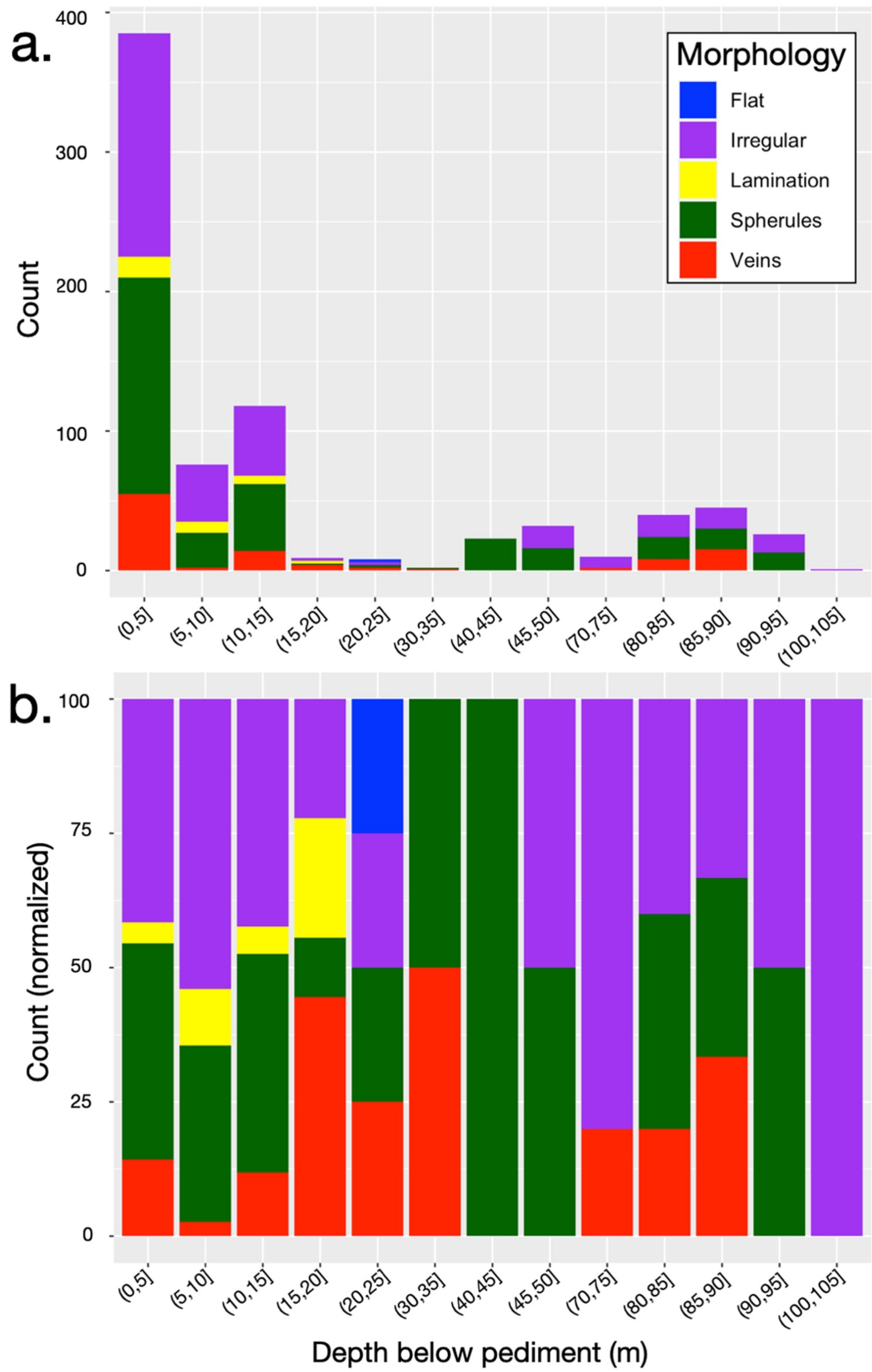

Figure 15. The count of features sorted by depth below the pediment (m) from 0 to 105 m. Bin size of 5 m. Note that elevation ranges with no features are omitted. (a) Total counts within that elevation range. (b) Normalized counts in that elevation range to highlight changes in proportions of different morphologies.

4. Discussion

4.1. Classes of Diagenetic Features

4.1.1. MAHLI Classification

All the types of diagenetic textures observed by Sun et al. (2019) were observed in the range of sols 1900–2900 except for dendrites. Irregular concretions were the most common type observed, followed by spherules, and these two types were often, but not always, found together. The primary location where irregular concretions are more abundant than spherules is in the transition from Jura to Knockfarril Hill. Flat textures are less common than spherules and irregular concretions at lower elevations but become the dominant morphology further into the Glasgow member. Darker flat nodular textures most closely resembling those seen in Sun et al. (2019) were only found in sols 3027–3036, while redder/lighter flat nodular textures were observed only two times, both in the VRR. Throughout the portion of the traverse examined here, veins were observed consistently, regardless of nodular texture presence.

The size of diagenetic features, measurable with MAHLI data, is also variable. The longest length and mean area of features is (Figure 9). The size of nodular features decreases with elevation except for an interval of large features along the Knockfarril Hill/Glasgow member boundary (Figure 10).

4.2. Complex Timing of Diagenetic Events in Gale Crater

On Earth, cementation along structural features results in complex and heterogeneous cementation patterns, with selective nodule cementation indicating an interaction between structure, fluid flow, and composition (Del Sole et al., 2020). Structural controls can affect porosity and permeability and therefore fluid flow, where structural characteristics can act as baffles to fluid flow and promote selective cementation along areas where fluid is able to flow leading to diagenesis being focused within compartments parallel to the structural bands (Del Sole et al., 2020). Alternately, there could be variation in diagenetic evolution due to variation in detrital composition (Mansurbeg et al., 2009).

The development of larger diagenetic nodules on Earth may be caused by a combination of increased porosity, slower flow rates/longer fluid residence time, increased temperature/pressure, and/or pore fluid ionic saturation. More reactive bedrock mineralogy may increase the ionic saturation so that bedrock ions can be dissolved into the pore space faster, freeing them up for diagenetic deposition. The presence of deformation features or high porosity/permeability can create subsurface pathways for fluid movement, concentrating the flow of mineral-rich fluids in certain areas. These pathways can lead to localized zones of mineral precipitation, forming nodules in clusters or layers (Del Sole et al., 2020), which can be further concentrated by compaction during burial.

Gale crater is a likely place for groundwater activity and emergence based on its regional location and depth (e.g., Horvath & Andrews-Hanna, 2017), which likely fueled the crater's long history of diagenesis even after the lacustrine phase was over. Primary depositional processes control porosity and permeability, which control how diagenetic processes progress. Higher in the section than the focus of this study, in the Mirador formation, different degrees of weathering were observed to be a proxy for cementation, where high permeability areas became better cemented and low permeability areas became poorly cemented (Banham et al., 2024; Meyer et al., 2024). This system results in good horizontal flow of fluids along bedding planes while impeding vertical diagenetic fluids (Banham et al., 2024).

4.2.1. The Vera Rubin ridge: Early Cementation and Limited Nodule Formation

The diagenetic nodules that we observed were sparse in VRR (Figure 7). Other studies have shown that VRR was subject to at least multiple-scales of diagenetic events that caused large-scale diagenetic modification largely in the form of cementation and recrystallization, leaving it strongly lithified and erosionally resistant (Bennett et al., 2021; Fraeman et al., 2020; Horgan et al., 2020). Our results are consistent with the interpretation that diagenetic modification was relatively early and decreased the area's porosity and permeability, reducing subsequent fluid flow and therefore limiting the nodules measured here compared to other strata we observed.

4.2.2. Glen Torridon: Early Pore Closure Due to Burial of Clay Mineral-Rich Sediment Limited Fluid Flow and Prohibited Formation of All Features Except Veins

Early diagenesis in VRR Jura member and GT Jura member rocks was perhaps similar, but during burial history the diagenetic pathways diverged significantly, with the remaining record difficult to discern which set of features developed first. In general, there were significantly fewer late diagenetic features (e.g., nodules) in the Knockfarril Hill members than elsewhere in Glen Torridon. This was especially true at the Glen Etive drill site (Figure 11e), where the lack of diagenetic features may indicate favorable conditions for the preservation of the organic material observed previously (Gasda et al., 2022; McAdam et al., 2022; O'Connell-Cooper et al., 2022).

The absence of all features except veins in Glen Torridon, spanning a large portion of Jura and Knockfarril Hill (Figures 3–8, 11), was likely driven by a decrease in porosity/permeability induced by the high abundance of clay minerals. Rudolph et al. (2022) proposed that the coarse sandstones of the pediment allowed for percolation of diagenetic fluids that were then impeded by the clay-rich impermeable Glen Torridon region. Our results are consistent with this if the fluid flow was top-down: a clay-rich package of strata may have formed an aquitard, slowing or impeding the flow of epidiagenetic groundwater off the pediment, due to its low permeability and porosity and leading to precipitation of larger features by increasing fluid residence time as well as pressure. Clays are also poor conductors of heat, so this could have retained heat in the area if the fluid was warm, encouraging larger nodules at the Knockfarril Hill-Glasgow boundary (Figure 8). In this situation, the water then had to move laterally to migrate around the Glen Torridon, allowing for more abundant and larger diagenetic features to form. The evidence presented here for top-down fluid migration may be a continuation of the top-down system explored in the context of Mg sulfate-bearing diagenetic fluids further upsection, controlled by grain size variations along a proposed unconformity (Bristow et al., 2021; Meyer et al., 2024; Seeger & Grotzinger, 2024). The observed nodule distribution in and above Glen Torridon suggests the basal circulation of a large groundwater system, which could either be isolated (defined by the pediment above and clays below) or the last phase of an environmentally significant sulfate-bearing fluid migration from much higher in the stratigraphy.

4.2.3. The Greenheugh Pediment

The depth of Mount Sharp group strata relative to the Greenheugh pediment (SPg unconformity) affects the location, size, and abundance of some of the nodule types (Figures 12–15). A high density of nodules (Figure 6) is strongly positively correlated with depth below the pediment (Table 2). The increase in feature size and density observed near the pediment is also highlighted by comparison with geomorphology (Fedo et al., 2022; Hughes, 2022). The transition from "smooth ridged" terrain to "fractured terrain" coinciding with an increase in diagenetic feature size and density upsection could be causal, where either diagenetic fluid flow fractured these rocks and created the diagenetic features or the rocks were more fractured for other reasons, thus allowing for increased diagenetic flow and subsequent nodule creation. In this case, Glen Torridon rocks may have been less affected by late-stage diagenesis.

We see a relationship between feature density within a scene and depth below the pediment (Table 2) but not with feature size (Table 3) that may have been driven by porosity, with a higher porosity allowing for more nodules forming in void space. Fluid ionic saturation and residence time may be the driving forces as they would affect feature size rather than density (Mansurbeg et al., 2009; Milliken & Olson, 2017; Weibel et al., 2023). Nodules form in clusters in areas where rock texture and fluid availability allow for their formation (Del Sole et al., 2020). A groundwater front may extend across tens of meters in thickness, influenced by local geological and hydrological conditions. High porosity and permeability result in a more diffuse groundwater front, while low porosity and permeability (including an aquitard) would result in a sharper and more defined front (Wright, 2007). If these diagenetic features were related to fluid paths influenced by the pediment, we would expect to see particular trends in diagenetic features close to the pediment with the intensity decreasing away from the pediment. In the 15 m below the Greenheugh pediment, we see a marked increase in total feature abundance (Figure 13a) and size (Figure 13b). While it is true that the rover drove along the base of the pediment for an extended period, the effect on feature size and the lack of the same signal when plotted against elevation (Figures 12 and 14) suggest a process linked to fluids influenced by the presence of the pediment/unconformity.

Lamination-enhancing features are only seen within 20 m depth below the pediment (Figure 15) and may have been deposited by the same fluid event that emplaced the pediment or a later fluid event that was upper bounded by the pediment. The same may go for the flat nodules, which are only seen at 20–25 m below the pediment

(Figure 15) and then disappear for ∼100 m (Figure 4). Lamination-enhancing and flat are statistically uncorrelated (Table 3).

The pediment appears to have formed via aeolian erosion, beveling off the front of Mount Sharp, with subsequent Stimson deposition and lithification preserving the beveled bedrock pedimentation surface as the basal SPg unconformity (Bryk et al., 2025). After these processes, several fluid events chemically altered the area near the SPg unconformity, and we propose that frequent nodules formed in this area. Unlike terrestrial pediments, the MSL team was unable to identify any evidence for erosional beveling by liquid water. Bryk et al. (2025) reported evidence for liquid water concentration along the unconformity in the form of soft sediment deformation (suggesting a presence of liquid water prior to lithification of the Stimson). However, most of the evidence for diagenetic alteration, such as systematic enrichment/depletion zones of mobile elements straddling the unconformity (Thompson et al., 2022), suggests fluid events that post-date lithification of the Stimson. We propose that the abundant nodules in this area formed during one or more of the later fluid events.

5. Conclusions

We tracked changes in diagenetic feature size, abundance, and morphology using Mastcam and MAHLI images. As noted in Sun et al. (2019), the stratigraphy of Mount Sharp continues to be diagenetically complex and likely affected by several distinct aqueous events that formed these nodules. We find that particularly notable changes in nodule morphology (Figures 5 and 7), size (Figures 8 and 9), and density (Figure 6) occurred at the Jura to Knockfarril Hill and Knockfarril Hill to Glasgow member boundaries.

The Jura to Knockfarril Hill transition hosts a sharp drop in diagenetic features. There are significantly fewer diagenetic features (e.g., nodules) in the Knockfarril Hill member than elsewhere in Glen Torridon, especially at the Glen Etive drill site, where the lack of diagenetic features may indicate favorable conditions for the preservation of organic material (Figure 11) (Gasda et al., 2022; McAdam et al., 2022; O'Connell-Cooper et al., 2022). The Knockfarril Hill to Glasgow transition included a return to abundant diagenetic nodules, with a spike in their size precisely at the member boundary (Figures 8 and 9).

We propose that these changes were strongly affected by the presence of the Greenheugh pediment. We found that there was no relationship between feature type/size and elevation (Figures 12 and 14), but a strong relationship between features and vertical distance from the pediment (Figures 13 and 15). The highest density of features was found immediately below the pediment and decreasing away from it, and the largest features were all clustered in the 10–15 m below the pediment bin. Lamination enhancing features were only seen within 20 m of the pediment surface and flat features only at 20 m from the pediment surface, so formation of these morphologies in particular could be related to events that took place along the unconformity. We propose that several diagenetic fluid flow events were able to flow along the SPg unconformity and form the variety of diagenetic features seen within 25 m of the unconformity. This likely created a setting in which increased residence time and possibly temperature led to the large and frequent diagenetic features observed at the Knockfarril Hill/Glasgow member boundary (Figure 8). We propose that several diagenetic fluid flow events were able to flow along the SPg unconformity and form the variety of diagenetic features seen within 25 m of the unconformity. This likely created a setting in which increased residence time and possibly temperature led to the large and frequent diagenetic features observed at the Knockfarril Hill/Glasgow member boundary (Figure 8).

Acknowledgments
We would like to acknowledge the entire Mars Science Laboratory team for collecting the data presented here and providing fruitful discussions. We would like to acknowledge funding from the Mars Science Laboratory Participating Scientist Program (80NSSC23K0189). A portion of this research was carried out at the Jet Propulsion Laboratory, California Institute of Technology, under a contract with the National Aeronautics and Space Administration (80NM0018D0004). Mastcam mosaics were processed by the Mastcam team at Malin Space Science Systems.

Data Availability Statement

Mastcam and MAHLI images used in this work are freely available from the PDS Geosciences Node: https://pds-geosciences.wustl.edu/missions/msl/index.htm, and the Planetary Data System Imaging Sciences node: https://pds-imaging.jpl.nasa.gov/volumes/msl.html. Analyst's Notebook can be found on the PDS at doi:10.17189/1520328.

References

Achilles, C. N., Rampe, E. B., Downs, R. T., Bristow, T. F., Ming, D. W., Morris, R. V., et al. (2020). Evidence for multiple diagenetic episodes in ancient fluvial-lacustrine sedimentary rocks in Gale Crater, Mars. *Journal of Geophysical Research: Planets*, *125*(8), e2019JE006295. https://doi.org/10.1029/2019JE006295

Anderson, R. B., & Bell, J. F., III. (2010). Geologic mapping and characterization of Gale Crater and implications for its potential as a Mars Science Laboratory landing site. *Mars*, *5*, 76–128. https://doi.org/10.1555/mars.2010.0004

Banham, S. G., Gupta, S., Cowart, A., & Author, C. D. (2024). *Diagenesis is controlled by primary aeolian depositional processes in the Mirador formation*. Abstract at LPSC.

Banham, S. G., Gupta, S., Rubin, D. M., Bedford, C. C., Edgar, L. A., Bryk, A. B., et al. (2022). Evidence for fluctuatingwind in shaping an ancient Martiandune field: The Stimson formation atthe Greenheugh pediment, Gale crater. *Journal of Geophysical Research: Planets*, *127*(9), e2021JE007023. https://doi.org/10.1029/2021je007023

Bennett, K. A., Fox, V. K., Bryk, A., Dietrich, W., Fedo, C., Edgar, L., et al. (2022). The curiosity rover's exploration of glen Torridon, Gale crater, Mars: An overview of the campaign and scientific results. *Journal of Geophysical Research: Planets*, *128*(1), e2022JE007185. https://doi.org/10.1029/2022JE007185

Bennett, K. A., Rivera-Hernández, F., Tinker, C., Horgan, B., Fey, D. M., Edwards, C., et al. (2021). Diagenesis revealed by fine-scale features at Vera Rubin ridge, Gale crater, Mars. *Journal of Geophysical Research: Planets*, *126*(5), e2019JE006311. https://doi.org/10.1029/2019JE006311

Bristow, T. F., Grotzinger, J. P., Rampe, E. B., Cuadros, J., Chipera, S. J., Downs, G. W., et al. (2021). Brine-driven destruction of clay minerals in Gale crater, Mars. *Science*, *373*(6551), 198–204. https://doi.org/10.1126/science.abg5449

Bryk, A. B., Dietrich, W. E., Bennett, K. A., Fox, V. K., Fedo, C. M., Lamb, M. P., et al. (2025). Pediment formation and subsequent erosion in Gale crater: Clues to the climate history of Mars. *Icarus*, *430*, 116445. https://doi.org/10.1016/j.icarus.2024.116445

Calef III, F. J., & Parker, T. (2016). MSL Gale merged Orthophoto mosaic [map]. *MSL Team; PDS Annex*. http://bit.ly/MSL_Basemap

Caravaca, G., Mangold, N., Dehouck, E., Schieber, J., Zaugg, L., Bryk, A. B., et al. (2022). From lake to river: Documentingan environmental transition across theJura/Knockfarril Hill members boundaryin the Glen Torridon region of Gale crater (Mars). *Journal of Geophysical Research: Planets*, *127*(9), e2021JE007093. https://doi.org/10.1029/2021JE007093

Cardenas, B. T., Grotzinger, J. P., Lamb, M. P., Lewis, K. W., Fedo, C. M., Bryk, A. B., et al. (2022). Barform deposits of the Carolyn Shoemaker formation, Gale crater, Mars. *Journal of Sedimentary Research*, *92*(12), 1071–1092. https://doi.org/10.2110/jsr.2022.032

David, G., Cousin, A., Forni, O., Meslin, P.-Y., Dehouck, E., Mangold, N., et al. (2020). Analyses of high-iron sedimentary bedrock and diagenetic features observed with ChemCam at Vera Rubin ridge, Gale crater, Mars: Calibration and characterization. *JGR: Planets*, *125*(10), e2019JE006314. https://doi.org/10.1029/2019JE006314

Dehouck, E., Cousin, A., Mangold, N., Frydenvang, J., Gasnault, O., Forni, O., et al. (2022). Bedrock geochemistry and alteration history of the clay-bearing Glen Torridon region of Gale crater, Mars. *Journal of Geophysical Research: Planets*, *127*(12), e2021JE007103. https://doi.org/10.1029/2021je007103

Del Sole, L., Antonellini, M., Soliva, R., Ballas, G., Balsamo, F., & Viola, G. (2020). Structural control on fluid flow and shallow diagenesis: Insights from calcite cementation along deformation bands in porous sandstones. *Solid Earth*, *11*(6), 2169–2195. https://doi.org/10.5194/se-11-2169-2020

Edgar, L. A., Fedo, C. M., Gupta, S., Banham, S. G., Fraeman, A. A., Grotzinger, J. P., et al. (2020). A lacustrine paleoenvironment recorded at Vera RubinRidge, Gale Crater: Overview of the sedimentology and stratigraphy observed by the Mars ScienceLaboratory curiosity rover. *Journal of Geophysical Research: Planets*, *125*(3), e2019JE006307. https://doi.org/10.1029/2019JE006307

Edgett, K. S., Yingst, R. A., Ravine, M. A., Caplinger, M. A., Maki, J. N., Ghaemi, F. T., et al. (2012). Curiosity's Mars hand lens imager (MAHLI) investigation. *Space Science Reviews*, *170*(1), 259–317. https://doi.org/10.1007/s11214-012-9910-4

Fedo, C. M., Bryk, A. B., Edgar, L. A., Bennett, K. A., Fox, V. K., Dietrich, W. E., et al. (2022). Geology and stratigraphic correlation of the Murray and Carolyn shoemaker formations across the glen Torridon region, Gale Crater, Mars. *Journal of Geophysical Research: Planets*, *127*(9), e2022JE007408. https://doi.org/10.1029/2022JE007408

Fedo, C. M., Grotzinger, J., Bryk, A., Bennett, K., Fox, V., Stein, N., et al. (2020). Ground-based stratigraphic correlation of the Jura and Knockfarril Hill members of the Murray formation, Gale crater: Bridging the Vera Rubin ridge – Glen Torridon divide.

Fedo, C. M., Grotzinger, J. P., Gupta, S., Fraeman, A., Edgar, L., Edgett, K., et al. (2018). *Sedimentology and stratigraphy OF the Murray formation* (Vol. 2083). GALE CRATER, MARS.2.

Fraeman, A. A., Arvidson, R. E., Catalano, J. G., Grotzinger, J. P., Morris, R. V., Murchie, S. L., et al. (2013). A hematite-bearing layer in Gale Crater, Mars: Mapping and implications for past aqueous conditions. *Geology*, *41*(10), 1103–1106. https://doi.org/10.1130/G34613.1

Fraeman, A. A., Edgar, L. A., Rampe, E. B., Thompson, L. M., Frydenvang, J., Fedo, C. M., et al. (2020). Evidence for a diagenetic origin of Vera Rubin ridge, Gale Crater, Mars: Summary and synthesis of Curiosity's exploration campaign. *Journal of Geophysical Research: Planets*, *125*(12), e2020JE006527. https://doi.org/10.1029/2020JE006527

Fraeman, A. A., Ehlmann, B. L., Arvidson, R. E., Edwards, C. S., Grotzinger, J. P., Milliken, R. E., et al. (2016). The stratigraphy and evolution of lower Mount Sharp from spectral, morphological, and thermophysical orbital data sets. *Journal of Geophysical Research: Planets*, *121*(9), 1713–1736. https://doi.org/10.1002/2016JE005095

Frydenvang, J., Gasda, P. J., Hurowitz, J. A., Grotzinger, J. P., Wiens, R. C., Newsom, H. E., et al. (2017). Diagenetic silica enrichment and late-stage groundwater activity in Gale crater, Mars. *Geophysical Research Letters*, *44*(10), 4716–4724. https://doi.org/10.1002/2017GL073323

Gasda, P. J., Comellas, J., Essunfeld, A., Das, D., Bryk, A. B., Dehouck, E., et al. (2022). Overview of the morphology and chemistry of diagenetic features in the clay-rich glen Torridon unit of Gale Crater, Mars. *Journal of Geophysical Research: Planets*, *127*(12), e2021JE007097. https://doi.org/10.1029/2021JE007097

Gasda, P. J., Comellas, J., Essunfeld, A., Das, D., Nellessen, M., Dehouck, E., et al. (2021). The chemistry and morphology of diagenetic features in glen Torridon, Gale crater. In *Lunar and planetary sciences Conference LII*.

Gwizd, S., Fedo, C., Grotzinger, J., Banham, S., Rivera-Hernández, F., Stack, K. M., et al. (2022). Sedimentological and geochemical perspectives on a marginal lake environment recorded in the Hartmann's Valley and Karasburg members of the Murray formation, Gale crater, Mars. *Journal of Geophysical Research: Planets*, *127*(8), e2022JE007280. https://doi.org/10.1029/2022je007280

Horgan, B. H. N., Johnson, J. R., Fraeman, A. A., Rice, M. S., Seeger, C., Bell, J. F., et al. (2020). Diagenesis of Vera Rubin ridge, Gale Crater, Mars, from Mastcam multispectral images. *Journal of Geophysical Research: Planets*, *125*(11), e2019JE006322. https://doi.org/10.1029/2019JE006322

Horvath, D. G., & Andrews-Hanna, J. C. (2017). Reconstructing the past climate at Gale crater, Mars, from hydrological modeling of late-stage lakes. *Geophysical Research Letters*, *44*, 8196–8204. https://doi.org/10.1002/2017GL074654

Hughes, M. N. (2022). Geomorphic map of glen Torridon in Gale crater, Mars. In *Digital research materials (data & supplemental files)* (Vol. 95). https://doi.org/10.7936/0cyw-3n10

Kah, L. C., Stack, K. M., Eigenbrode, J. L., Yingst, R. A., & Edgett, K. S. (2018). Syndepositional precipitation of calcium sulfate in Gale Crater, Mars. *Terra Nova*, *30*(6), 431–439. https://doi.org/10.1111/ter.12359

Knight, A. L., Mitra, K., & Catalano, J. G. (2024). Transformation of Precursor iron(III) minerals in diagenetic fluids: Potential origin of gray hematite at Vera Rubin ridge. *JGR Planets*, *129*, 4. https://doi.org/10.1029/2023JE007931

Kronyak, R. E., Kah, L. C., Edgett, K. S., VanBommel, S. J., Thompson, L. M., Wiens, R. C., et al. (2019). Mineral-filled fractures as indicators of multigenerational fluid flow in the Pahrump Hills member of the Murray formation, Gale crater, Mars. *Earth and Space Science*, *6*(2), 238–265. https://doi.org/10.1029/2018EA000482

Malin, M. C., Ravine, M. A., Caplinger, M. A., Ghaemi, F. T., Schaffner, J. A., Maki, J. N., et al. (2017). The Mars science laboratory (MSL) Mast cameras and descent imager: Investigation and instrument descriptions. *Earth and Space Science*, *4*(8), 506–539. https://doi.org/10.1002/2016EA000252

Manelski, H. T., Sheppard, R. Y., Fraeman, A. A., Wiens, R. C., Johnson, J. R., Rampe, E. B., et al. (2023). Compositional variations in sedimentary deposits in Gale Crater as observed by ChemCam passive and active spectra. *Journal of Geophysical Research: Planets*, *128*(3), e2022JE007706. https://doi.org/10.1029/2022JE007706

Mansurbeg, H., Caja, M. A., Marfil, R., Morad, S., Remacha, E., Garcia, D., et al. (2009). Diagenetic evolution and porosity destruction of turbiditic hybrid arenites and siliciclastic sandstones of foreland basins: Evidence from the eocene hecho group, pyrenees, Spain. *Journal of Sedimentary Research*, *79*(9), 711–735. https://doi.org/10.2110/jsr.2009.060

Martin, P. E., Farley, K. A., Baker, M. B., Malespin, C. A., Schwenzer, S. P., Cohen, B. A., et al. (2017). A two-step K-Ar experiment on Mars: Dating the diagenetic formation of jarosite from amazonian groundwaters. *Journal of Geophysical Research: Planets*, *122*(12), 2803–2818. https://doi.org/10.1002/2017JE005445

McAdam, A. C., Sutter, B., Archer, P. D., Franz, H. B., Wong, G. M., Lewis, J. M. T., et al. (2022). Evolved gas analyses of sedimentary rocks from the glen Torridon clay-bearing unit, Gale crater, Mars: Results from the Mars science laboratory sample analysis at Mars instrument suite. *Journal of Geophysical Research: Planets*, *127*(9), e2022JE007179. https://doi.org/10.1029/2022je007179

Meyer, M. J., Milliken, R. E., Stack-Morgan, K. M., Edgar, L. A., Rampe, E. B., Turner, M. L., et al. (2024). The geological context and significance of the clay-sulfate transition region in Mount Sharp, Gale Crater, Mars: An integrated assessment based on orbiter and rover data. *GSA Bulletin*, *137*(1–2), 82–115. https://doi.org/10.1130/B37355.1

Milliken, K. L., & Olson, T. (2017). Silica Diagenesis, Porosity Evolution, and Mechanical Behavior In Siliceous Mudstones, Mowry Shale (Cretaceous), Rocky Mountains, U.S.A. *Journal of Sedimentary Research*, *87*(4), 366–387. https://doi.org/10.2110/jsr.2017.24

Milliken, R. E., Grotzinger, J. P., & Thomson, B. J. (2010). Paleoclimate of Mars as captured by the stratigraphic record in Gale Crater. *Geophysical Research Letters*, *37*(4), L04201. https://doi.org/10.1029/2009GL041870

Nachon, M., Clegg, S. M., Mangold, N., Schröder, S., Kah, L. C., Dromart, G., et al. (2014). Calcium sulfate veins characterized by ChemCam/Curiosity at Gale Crater, Mars. *Journal of Geophysical Research: Planets*, *119*(9), 1991–2016. https://doi.org/10.1002/2013JE004588

Nachon, M., Mangold, N., Forni, O., Kah, L. C., Cousin, A., Wiens, R. C., et al. (2017). Chemistry of diagenetic features analyzed by ChemCam at Pahrump Hills, Gale crater, Mars. *Icarus*, *281*, 121–136. https://doi.org/10.1016/j.icarus.2016.08.026

O'Connell-Cooper, C. D., Thompson, L. M., Spray, J. G., Berger, J. A., Gellert, R., McCraig, M., et al. (2022). Statistical analysis of APXS-derived chemistry of the clay-bearing Glen Torridon region and Mount Sharp group, Gale crater, Mars. *Journal of Geophysical Research: Planets*, *127*(9), e2021JE007177. https://doi.org/10.1029/2021JE007177

Rampe, E. B., Bristow, T. F., Morris, R. V., Morrison, S. M., Achilles, C. N., Ming, D. W., et al. (2020). Mineralogy of Vera Rubin ridge From the Mars Science Laboratory CheMin Instrument. *Journal of Geophysical Research: Planets*, *125*(9), e2019JE006306. https://doi.org/10.1029/2019JE006306

Rudolph, A., Horgan, B., Johnson, J., Bennett, K., Haber, J., Bell, J. F., et al. (2022). The distribution of clay minerals and their impact on diagenesis in Glen Torridon, Gale crater, Mars. *Journal of Geophysical Research: Planets, Glen Torridon Special Issue 2021*, *127*(10), e2021JE007098. https://doi.org/10.1029/2021je007098

Seeger, C. H., & Grotzinger, J. P. (2024). *Diagenesis of the Clay-Sulfate Stratigraphic Transition*. Mount Sharp Group, Gale Crater.

Sheppard, R. Y., Thorpe, M. T., Fraeman, A. A., Fox, V. K., & Milliken, R. E. (2021). Merging Perspectives on Secondary Minerals on Mars: A Review of Ancient Water-Rock Interactions in Gale Crater Inferred from Orbital and In-Situ Observations. *Minerals*, *11*(9), 986. Article 9. https://doi.org/10.3390/min11090986

Stack, K. M., Grotzinger, J. P., Kah, L. C., Schmidt, M. E., Mangold, N., Edgett, K. S., et al. (2014). Diagenetic origin of nodules in the Sheepbed member, Yellowknife Bay formation, Gale crater, Mars. *Journal of Geophysical Research: Planets*, *119*(7), 1637–1664. https://doi.org/10.1002/2014JE004617

Sun, V. Z., Stack, K. M., Kah, L. C., Thompson, L., Fischer, W., Williams, A. J., et al. (2019). Late-stage diagenetic concretions in the Murray formation, Gale crater, Mars. *Icarus*, *321*, 866–890. https://doi.org/10.1016/j.icarus.2018.12.030

Sutter, B., McAdam, A. C., Wong, G. M., Clark, J. V., Archer, P. D., Franz, H. B., et al. (2022). Constraining alterationprocesses along the Siccar Point groupunconformity, Gale crater, Mars: Resultsfrom the sample analysis at Marsinstrument. *Journal of Geophysical Research: Planets*, *127*(11), e2022JE007387. https://doi.org/10.1029/2022je007387

Thompson, L. M., Spray, J. G., O'Connell-Cooper, C., Berger, J. A., Yen, A., Gellert, R., et al. (2022). Alteration at the base of the Siccar Point unconformity and further evidence for an alkaline provenance at Gale Crater: Exploration of the Mount Sharp group, Greenheugh pediment cap rock contact with APXS. *Journal of Geophysical Research: Planets*, *127*(11), e2021JE007178. https://doi.org/10.1029/2021JE007178

Vasavada, A. R. (2022). Mission Overview and Scientific Contributions from the Mars Science Laboratory Curiosity Rover After Eight Years of Surface Operations. *Space Science Reviews*, *218*(3), 14. https://doi.org/10.1007/s11214-022-00882-7

Watkins, J. A., Grotzinger, J. P., Stein, N. T., Banham, S. G., Gupta, S., Rubin, D. M., et al. (2022). Burial and exhumation of sedimentary rocks revealed by the base Stimson erosional unconformity, Gale crater, Mars. *Journal of Geophysical Research: Planets*, *127*(7), e2022JE007293. https://doi.org/10.1029/2022je007293

Weibel, R., Vosgerau, H., Larsen, M., Guarnieri, P., Kokfelt, T. F., Dideriksen, K., et al. (2023). Diagenetic effect on reservoir quality of siliciclastic and volcaniclastic sandstones from a Paleogene volcanic rifted margin, East Greenland. *Journal of Sedimentary Research*, *93*(12), 895–931. https://doi.org/10.2110/jsr.2021.127

Wright, V. P. (2007). Calcrete. In D. J. Nash & S. J. McLaren (Eds.), *Geochemical Sediments and Landscapes* (pp. 10–45). Blackwell Publishing.

Yingst, R. A., Cowart, A. C., Kah, L. C., Gupta, S., Stack, K., Fey, D., et al. (2023). Depositional and Diagenetic Processes of Martian Lacustrine Sediments as Revealed at Pahrump Hills by the Mars Hand Lens Imager, Gale Crater, Mars. *JGR: Planets*, *128*(5), e2022JE007394. https://doi.org/10.1029/2022JE007394

Zucker, M. (2021). Point Picker.